Environmental Science: Atmospheres

ROYAL SOCIETY OF CHEMISTRY

PAPER

View Article Online
View Journal

Cite this: DOI: 10.1039/d5ea00159e

Nocturnal vertical gradients in O_3, PAN and PAA in a boreal forest: the role of chemical reactions, deposition and entrainment

Simone T. Andersen, *[a] Carolina Nelson, [a] Laura Wüst,[a] Patrick Dewald, [a] Gunther N. T. E. Türk,[a] Jan Schuladen,[a] Horst Fischer,[a] Mikael Ehn,[b] Tuukka Petäjä, [b] Üllar Rannik,[b] Ilona Ylivinkka, [bc] Lauri R. Ahonen,[bc] Robby Rynek, [d] Helko Borsdorf, [d] Thomas Mayer,[d] Jos Lelieveld[a] and John N. Crowley *[a]

The complex interplay between different processes (physical losses, chemical losses and entrainment) defines the vertical gradient of many trace gases in forested environments. Despite this, height-resolved measurements of trace gases within a forest canopy are scarce. We present measurements of O_3, PAN (peroxy acetyl nitric anhydride, $CH_3C(O)OONO_2$), and PAA (peroxy acetic acid, $CH_3C(O)OOH$) at 6 heights between 1 and 28 m above and below the canopy at the SMEAR II site in the Finnish boreal forest. Through analysis of O_3, PAN, and PAA nocturnal time-series we derived their height-dependent net loss rate coefficients. The net lifetimes of O_3, PAN and PAA were highly variable with values of 1.5–42 h, 1.0–29 h, and 0.7–15 h, respectively, with the shortest lifetimes often measured at the lowest heights. The relative loss rates of PAN or PAA compared to O_3 (k_{PAN}/k_{O_3} and k_{PAA}/k_{O_3}) varied between 1.0–3.0 (85% of the measurements) and 1.0–5.0 (78% of the measurements) with medians of 1.7 and 2.4, respectively. The physical loss of O_3, PAN and PAA was the major loss process (>90%), with chemical losses playing only a minor role. Entrainment significantly compensated for the physical and chemical losses and led to reduced net loss values of each trace gas, with exceptions encountered on a few nights when the sub-canopy and above-canopy air masses were decoupled as a result of *e.g.* low wind speed and friction velocity. Our vertical profiles of O_3, PAN, and PAA reveal the complex interplay of boundary layer dynamics and chemistry at this forested location.

Received 26th November 2025
Accepted 17th March 2026

DOI: 10.1039/d5ea00159e

rsc.li/esatmospheres

Environmental significance

O_3 and PAN are centrally important trace gases in the atmosphere. The complex interplay between their physical losses, chemical losses and entrainment defines their vertical gradient through ground level to above canopy in forested environments. We present measurements of O_3, PAN, (and PAA) at 6 heights above and below the canopy in the Finnish boreal forest. Through analysis of O_3, PAN, and PAA nocturnal time-series at all 6 heights we show that entrainment and physical losses are the dominant processes impacting the shape of the gradient, however, chemical loss processes become non-negligible close to the ground due to soil emissions of NO.

1 Introduction

This study focuses on the atmospheric chemistry of ozone (O_3), peroxy acetyl nitric anhydride ($CH_3C(O)OONO_2$, commonly known as PAN), and peroxy acetic acid ($CH_3C(O)OOH$, PAA) at nighttime in a boreal forest. O_3 is a phytotoxic trace-gas which is generated photochemically in the troposphere and is an important component of photochemical smog, a precursor for the hydroxyl radical (OH)[1] and an important oxidant of biogenic volatile organic compounds (BVOCs).[2] PAN has been shown to be an important source of NO_x in remote areas (where few direct sources exist), notably in the boundary layer, through long-range transport followed by thermal decomposition.[3–5] PAA formation is a sink of peroxy acetyl radicals ($CH_3C(O)O_2$, PAN precursor) and HO_x (hydroxyl radicals (OH) + hydroperoxyl radicals (HO_2)).

PAA measurements in forested (non-biomass burning influenced) regions are limited to a few previous studies,[6–8] with data obtained at one height. Although O_3 and PAN have been measured frequently in forested regions, the observations are often limited to three measurement strategies; (1)

[a]Atmospheric Chemistry Department, Max-Planck-Institute for Chemistry, 55128-Mainz, Germany. E-mail: simone.andersen@mpic.de; john.crowley@mpic.de
[b]Institute for Atmospheric and Earth System Research (INAR)/Physics, Faculty of Science, University of Helsinki, Helsinki 00014, Finland
[c]Station for Measuring Ecosystem – Atmosphere Relations II (SMEAR II), University of Helsinki, Korkeakoski, 35500, Finland
[d]Department of Monitoring and Exploration Technologies, Helmholtz-Centre for Environmental Research – UFZ, Permoserstraße 15, 04318 Leipzig, Germany

concentration at one height within the canopy or sub-canopy,[6,9] (2) concentration at one height within the canopy/sub-canopy and one above the tree tops[10] or (3) flux measurements conducted above the tree tops.[11,12] While these approaches give information about the chemistry and meteorology influencing measurements at single heights, they do not provide a detailed picture of gradients (and controlling factors) from the ground to above the canopy.

Height dependent O_3 mixing ratios have previously been measured at SMEAR II (Station for Measuring Ecosystem–Atmosphere Relations II),[13,14] though the data was restricted to three heights between 4 and 17 m (the remaining heights were above the tree tops)[15] and were therefore blind to processes taking place close to the surface. To explain nocturnal gradients in O_3 (or other trace gases) the chemical and physical loss terms (L) as well as the source term (S) from entrainment of above-canopy O_3 rich air would have to be evaluated at different heights when assuming horizontal homogeneity in the forest as described in eqn (1), where k_{ent}, k_{phys}, and k_{chem} are the entrainment rate coefficient, the rate coefficient for physical losses, and the chemical loss coefficient, respectively. $[C]_{above}$ and $[C]_h$ are the concentrations of compound C above the canopy and at height h. Entrainment and physical losses (deposition) are discussed further below and chemical losses of each molecule are described in detail together with the results.

$$\frac{d[C]_h}{dt} = S - L = k_{ent}[C]_{above} - \left(k_{phys_h}[C]_h + k_{chem_h}[C]_h\right) \quad (1)$$

The vertical mixing of air within the stable nighttime boundary layer and also the development of temperature inversions and the degree of coupling of the sub-canopy air with that above are largely controlled by the friction velocity which is related to the horizontal wind speed.[16–20] At the SMEAR II site, it has been shown that decoupling of above-canopy and sub-canopy air at nighttime has a large impact on in-canopy, net O_3 loss rates[21] highlighting the fact that entrainment has a strong influence on the composition of sub-canopy air in forested regions.

The uptake of a trace-gas to a surface (*i.e.* deposition) is controlled both by the rate of transport to the surface (the transport resistance) and its accommodation and further degradation at the surface (the surface resistance) (see Seinfeld,[22] Section 16.4). While the transport resistance depends largely on turbulence (*i.e.* vertical exchange rates) and is essentially the same for all trace gases, the surface resistance varies depending on what surface (soil, vegetation, water) it deposits on. Deposition to vegetation occurs at the surface of the leaf (cuticle) and through the stomata. The deposition resistance to vegetation can therefore be split into the resistance to deposit to the surface (cuticular resistance) and a combination of the stomatal resistance and the mesophyllic resistance (resistance due to processes taking place inside the leaf, which slow stomatal deposition down).[23,24] Cuticular uptake depends on the surface characteristics of the leaf (leaf surface area, leaf pubescence, waxes and exudates on the leaf surface, and leaf wetness) as well as the chemical characteristics of the trace gas.[24] O_3 deposition to foliage has previously been studied at the SMEAR II site using flux measurements (eddy covariance and gas-exchange enclosure) and modelling.[25,26] Altimir *et al.*[25] showed that at a relative humidity lower than 70% (RH where water films start to grow on leaves/needles) the predicted stomatal O_3 deposition could explain the behaviour in measured O_3 deposition, however, when the relative humidity was higher than 70% the prediction underestimated the observed behaviour, which showed increasing non-stomatal (cuticular) uptake with increasing relative humidity. Furthermore, in addition to deposition onto vegetation, trace gases can also deposit onto soil, whose water content can modify the surface resistance depending on whether the trace gas is soluble. The solubility of a trace gas is described by the Henry's law solubility constant and the degree of surface wetness can be related to the relative humidity.[25] For gases with intermediate solubilities, we would therefore expect the surface resistance to play a role and the rate of dry deposition to depend on relative humidity.

In this study, we have conducted measurements at several heights between 1 and 28 m (6 heights within the canopy and sub-canopy, and 1 above the tree-tops) for three weeks at the SMEAR II site at the Hyytiälä Forest Station. Nighttime measurements of O_3, PAN and PAA loss rates have been used to investigate the height-dependent chemical and physical loss terms as well as the role of entrainment of above canopy air in controlling mixing ratios of these trace gases and their vertical gradients. We only analyse nighttime measurements in order to reduce the chemical complexity (in the absence of photochemistry).

2 Methodology

2.1 Campaign description

The BAIRN-VIP (Biosphere–Atmosphere Interactions and the Reactive Nitrogen Budget: VertIcal Profiles of Key Species) campaign took place at the SMEAR II site at the Hyytiälä Forest Station, Finland, between August 25th and September 27th 2024. The daytime temperatures decreased from a maximum ~25 °C at the beginning of the campaign to ~10–15 °C at the end of the campaign. The first half of the campaign was dominated by sunny and dry days although the relative humidity reached 100% within the canopy on several nights, which was a stark contrast to the second half, which was cloudier with episodes of significant rainfall.

An overview of the layout of the instruments operated by the Max Planck Institute is shown in Fig. 1. Photolysis frequencies, nitrate radicals (NO_3) and nitrogen pentoxide (N_2O_5) were measured from a container on top of a 35 m tower located in a clearing. The forest surrounding the clearing is dominated by Scots pine trees with a tree-top around 20–22 m.[17,27] The sum of monoterpenes was measured by the University of Helsinki at the top of the tower at 36 m and speciated monoterpenes were measured by the Helmholtz-Centre for Environmental Research (UFZ) at the same height for 48 hours during the campaign. Temperature and humidity sensors were attached to the tower at 7 different heights between 2 and 32 m (see caption for

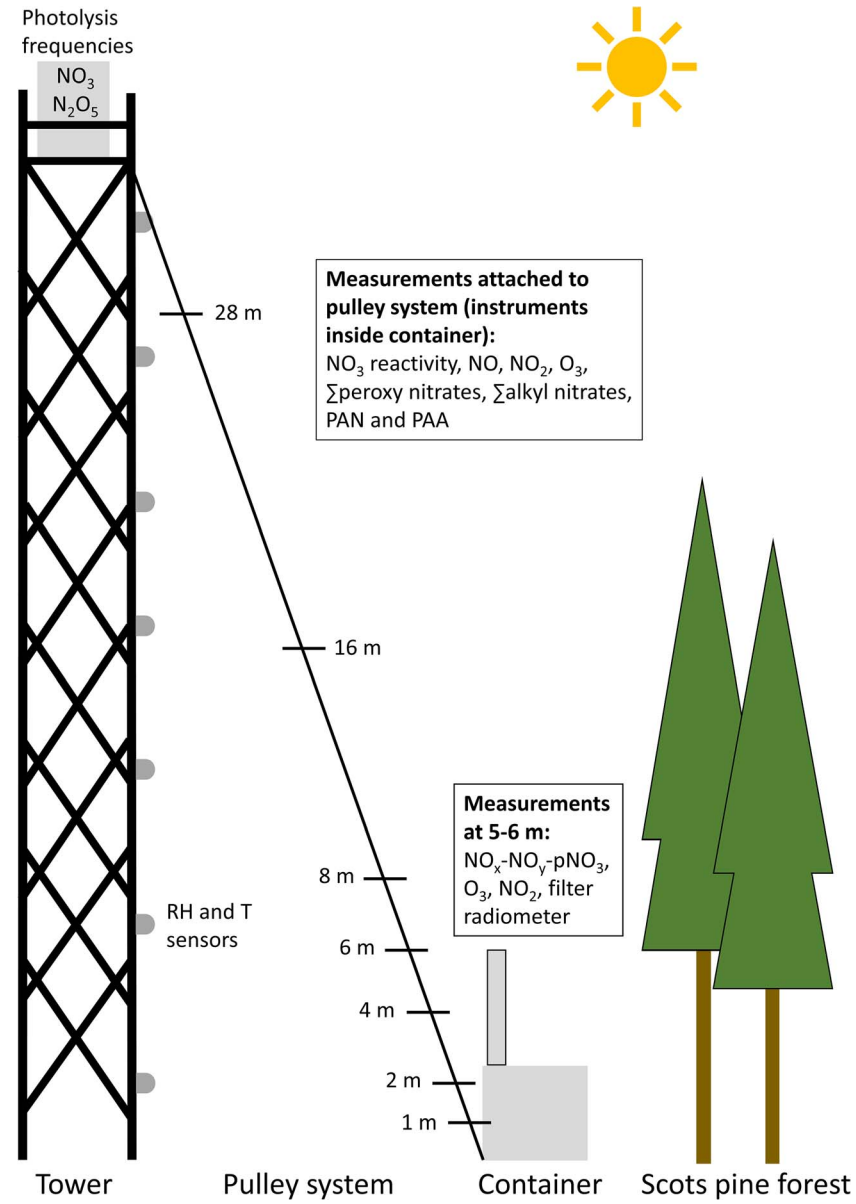

Fig. 1 Schematic showing the instrument and inlet locations during BAIRN-VIP. The inlet heights were 1, 2, 4, 6, 8, 16 and 28 m. The approximate, average tree-top height was ~20–22 m. The stationary, temperature and relative humidity (RH) sensors were at heights of 2, 7, 12, 17, 22, 27 and 32 m agl.

details) and augmented the measurements of the same parameters at 11 heights between 0.4 and 125 m on the 128 m mast in the forest which are operated continuously throughout the year. O_3, nitrogen dioxide (NO_2), NO_x (NO_2 + NO (nitrogen oxide)), the sum of nitrogen containing species ($\sum NO_y$), particulate nitrate (pNO_3), and total solar radiation were measured at 3–6 m above the ground from the top of a container located directly next to the tower. Vertical gradient measurements within the clearing were obtained using an automated pulley system which varied the height of a set of inlets attached (*via* ~35 m of 1/4-inch (outer diameter) PFA tubing) to instruments measuring NO, NO_2, O_3, NO_3 reactivity, PAN, PAA, NO_x, the sum of peroxy nitric anhydrides ($\sum$PANs), and the sum of alkyl nitrates ($\sum$ANs). Between September 6th and 17th 2024, the inlets cycled between 6 heights (1, 2, 4, 8, 16, and 28 m) for 7 min at each height. From September 17th until the end of the campaign measurements at 6 m were added to the cycle and the time at each height was reduced to 6 min to maintain the total cycle time of 42 minutes excluding time to change height. The pulley automation was occasionally deactivated to examine the time evolution of trace gases at a single height over a longer period. The measurements used in this study are described in detail in Section 2.2.

2.2 Measurements

2.2.1 Fixed height measurements. O_3 was measured at a fixed height of approximately 5 m (on top of the container) with a commercial instrument (2B Technologies model 205)

using UV absorption at ~254 nm. The limit of detection (LOD) is 2 ppbv (part per billion by volume) for 10 s averaging time.

Temperature and relative humidity were recorded by a commercial weather station (DNT000008) and additional portable sensors which were attached to the tower at 2, 7, 12, 17, 22, 27, and 32 m above the ground. An additional sensor, which measures temperature, relative humidity, and pressure, was attached 50 cm above the inlets on the pulley system. Temperature and relative humidity were additionally measured on the 128 m mast inside the forest (part of the SMEAR II dataset) at 0.4, 1.5, 3.3, 5.8, 8.8, 12.5, 16.8, 21.6, 27.0, 67.2, and 125 m, and wind speed was measured at 8.4, 16.8, 33.6, 67.2, and 125 m using 2D ultrasonic anemometers. It should be noted that the heights on the mast and the tower are not directly equivalent as the elevation of the ground differs by a few meters. Time series of the temperature and relative humidity measurements on the tower and mast are plotted in Fig. S1 and S2 and agree well for similar heights.

A spectral radiometer (Metcon Gmbh) was installed at 38 m (on top of the tower) to measure the actinic flux, which was used to calculate photolysis frequencies as described elsewhere.[28] Total solar radiation was measured at 5 m by the commercial weather station described above. The NO_2 photolysis frequency (J_{NO_2}) at 38 m was used to calculate a value at 5 m by scaling to the ratio of total solar radiation at 5 m and J_{NO_2} when both sensors were in direct sunlight.

A Vocus PTR-TOF (proton transfer reaction – time of flight) mass spectrometer (Tofwerk 2R) was used to measure the sum of monoterpenes ($\sum$MT) at 36 m during the campaign. Blank measurements and calibrations, using a National Physical Laboratory (NPL) 20 component PTR-MS standard, were performed 7 times per day during the measurement period. Speciated monoterpenes were only measured for 48 hours of the campaign (September 10–12th) by sampling for 4 hours onto Bio-Monitoring sorbent tubes followed by analysis with thermal desorption-gas chromatography-mass spectrometry (TD-GC-MS) as described by Rynek *et al.*[29]

2.2.2 Vertical gradient measurements. Vertical gradients of O_3 were measured with a second commercial instrument (2B Technologies model 205) using UV absorption at ~254 nm, which also has a LOD of 2 ppbv for 10 s averaging time. Timeseries of the measured O_3 at different heights are plotted in Fig. S3. The O_3 measurement on the pulley has been compared (Fig. S4) to those measured on top of the container, when the pulley instrument was measuring at 4–6 m. The O_3 mixing ratios generally agreed well with each other throughout the campaign (slope of 1.03), which also indicates that losses of O_3 throughout the 35 m inlet line are negligible. In addition, the two instruments were cross calibrated in the laboratory, and the one on the container was compared to O_3 measurements using a 1.2 m absorption cell with a 254 nm light source (low pressure mercury lamp).

NO and NO_2 were measured using a two-channel chemiluminescence instrument with a modified blue light converter (BLC, Droplet Measurement Technologies 2005) for detection of NO_2 as described in Nussbaumer *et al.*[30] The sensitivity of each channel was calibrated every 2–3 days, and the conversion efficiency of the BLC (33 ± 1.5%) was calibrated 4 times during the campaign and remained stable. The sensitivity of the instrument was corrected for fluorescence quenching by water vapour using a calibration performed in the laboratory in which the relative humidity was systematically varied between 0 and 100%. The LOD of NO was calculated as 3σ of the zero measurements to be 4.5 pptv (parts per trillion by volume) for 1 min averaging time, and the total measurement uncertainty (TMU) was 4.5 pptv + 4%. For NO_2 the LOD was calculated as a combination of the 3σ of the zero measurements for both channels and converted into NO_2 using the conversion efficiency, resulting in 17 pptv and a TMU of 17 pptv + 5%.

The ambient reactivity of NO_3 towards biogenic volatile organic compounds (BVOCs) was quantified by a cavity ring-down spectroscopy (CRDS) measurement (at 662 nm) of synthetic NO_3 when mixed with either synthetic or ambient air in a flow-tube.[31] A numerical simulation procedure, which *e.g.* takes reactions of NO_3 with NO_2 and reversible formation of N_2O_5 into account and has been described in detail by Liebmann *et al.*,[31] was used to correct the measurements for competing reactions taking place inside the flow-tube in order to extract the VOC contribution to the measured NO_3 consumption. The average LOD during the campaign was 0.006 s^{-1}. A detailed analysis of the NO_3 reactivity data from the campaign is given in Dewald *et al.*[32]

PAN and PAA were measured using an Iodide Chemical Ionisation Mass Spectrometer (I-CIMS). Briefly, the original instrument was developed at Georgia Tech by THS and is the same as that described in Phillips *et al.*,[7] amended for aircraft use as described in Dörich *et al.*[33] and with the I^- ions generated using a VUV photoionization source (Heraeus, Type PKS106) instead of polonium.[34] Both PAN and PAA were detected as $CH_3C(O)O^-$ at m/z 59. PAN is thermally decomposed (at *ca.* 150 °C) to $CH_3C(O)O_2$ and NO_2 in a heated PFA inlet (R1) before $CH_3C(O)O_2$ reacts with I^- in the ion-molecule-reactor (IMR) to generate $CH_3C(O)O^-$ (R2). PAA is directly converted into $CH_3C(O)O^-$ by reaction with the I^- ions in the IMR (R3).

$$CH_3C(O)OONO_2 + \Delta \rightarrow CH_3C(O)OO + NO_2 \quad (R1)$$

$$CH_3C(O)O_2 + I^- \rightarrow CH_3C(O)O^- + IO \quad (R2)$$

$$CH_3C(O)OOH + I^- \rightarrow CH_3C(O)O^- + HOI \quad (R3)$$

A datapoint at m/z 59 was obtained every *ca.* 8 seconds. To separate the signals from PAN and PAA at m/z 59, NO was added periodically (3 min of PAN measurements followed by 3 min of PAA measurements) to the heated inlet removing the $CH_3C(O)O_2$ generated from the thermal decomposition of PAN (R1) and thereby removing the sensitivity to PAN. The signal due to PAA at each height was determined as the average of all the measurements at one height during a measurement cycle where PAN was titrated, while the signal due to PAN was determined by subtracting the median titrated signal (from PAA plus any background signal) at a given height from the untitrated signal measured at the same height during a measurement cycle

before taking an average. The background signal was measured every 70 minutes and interpolated.

The PAN signal was converted to a mixing ratio by reference to calibrations performed approximately every 70 minutes for 5 minutes using a C^{13}-acetone-based, photochemical, calibration source.[35,36] C^{13}-PAN, which was detected at m/z 61, was preferred to C^{12}-PAN as previously used to avoid memory effects on m/z 59. The time-dependent PAN sensitivity was derived from interpolating between calibrations. A gradual decrease in the sensitivity was observed during the campaign, however, only very small variations were observed between individual calibrations.

The I-CIMS sensitivity to PAA was determined 3 times during the campaign by bubbling (for ~50–160 min) a flow of PAA from a diffusion source containing 37% PAA in acetic acid through a solution of acidified (2.5×10^{-3} M H_2SO_4) potassium iodide (KI, 0.3 mol L^{-1}) and simultaneously to the inlet of the I-CIMS. PAA oxidises I^- to I_3^- ((R4) and (R5)) which, after transfer from the bubbler to a 3 cm UV-cuvette, was quantified by its optical absorption in the wavelength range ~280 to 400 nm using the extinction coefficients reported by Awtrey and Connick.[37] A separate set of laboratory experiments, in which a known amount of iodine was stoichiometrically converted (*via* reaction with iodide) to I_3^- confirmed the accuracy of the spectrum of Awtrey and Connick.[37]

$$CH_3C(O)OOH + 2I^- + 2H^+ \rightarrow CH_3C(O)OH + I_2 + H_2O \quad (R4)$$

$$I_2 + I^- \rightleftharpoons I_3^- \quad (R5)$$

This calibration procedure assumes that only PAA oxidises I^- to I_3^- and that the scavenging efficiency of the bubbler was 100%. A potential further oxidant for I^- is hydrogen peroxide (H_2O_2) which is present in the PAA sample manufactured by mixing H_2O_2 with acetic acid ($CH_3C(O)OH$):

$$CH_3C(O)OH + H_2O_2 \rightleftharpoons H_2O + CH_3C(O)OOH \quad (R6)$$

Previous work from this laboratory has shown that the headspace above the PAA samples used contains only ~1% H_2O_2 compared to PAA, reflecting its lower vapour pressure.[38] Experiments in which two bubblers in series were used revealed no measurable signal from I_3^- in the second bubbler, indicating that the scavenging efficiency was >95%. The reproducibility of the 3 calibrations performed during the campaign was within 6% (1 standard deviation, σ).

The PAA sensitivity in the I-CIMS has been shown to be highly humidity dependent[7] with decreasing sensitivity with increasing humidity. Corrections were therefore applied using the relative humidity, temperature and pressure measurements from the pulley system. Timeseries of the measured PAN and PAA at different heights are plotted in Fig. S5 and S6. Neither PAN nor PAA have irreversible losses to PFA tubing, so we do not expect any losses through the sampling lines.

2.3 Atmospheric stability calculations

Atmospheric stability for the SMEAR II site has previously been studied by Peltola *et al.*,[39] who defined a universal meteorological decoupling parameter Ω, which can be used to identify periods when the sub-canopy flow is decoupled from the rest of the surface layer above the tree tops. When $\Omega > 0.59$, the sub-canopy flow is coupled and entrainment from above occurs.[17] For $0.59 > \Omega > 0.43$, the sub-canopy is weakly decoupled, which can lead to a reduction in entrainment. And when $\Omega < 0.43$, the sub-canopy is clearly decoupled from above resulting in a strong reduction in entrainment. A detailed description of how Ω was calculated for BAIRN-VIP using meteorological measurements from the 128 m mast is given in Dewald *et al.*[32] and will not be repeated here.

3 Results and discussion

During the BAIRN-VIP campaign a total of 33 vertical gradients (1–28 m) of O_3, PAN and PAA were measured throughout the diel-cycle. The vertical gradients of all the trace gases discussed here displayed great variability, with different gradients obtained at day and at night, as well as between different nights and also during different periods of the same night. Large variations in O_3 gradients have been observed at this site for many years,[15] but this is to our knowledge the first time for PAN and PAA.

Fig. 2 shows examples of vertical gradients at the beginning and end of three different nights. On the night from the 10–11th September, O_3, PAN and PAA (panels A, B, and C) display no or only weak vertical gradients at the beginning of the night (orange circles and solid lines) which switch to stronger vertical gradients (orange/red triangles and dashed lines) at the end of the night. This transition is accompanied by a change in the absolute values of the vertical gradients of temperature and relative humidity (panels D and E).

For the nights 8–9th September (blue) and 15–16th September (grey) large temperature inversions (panel D) can be observed from the beginning (circles and solid lines) of the night, which results in gradients in O_3, PAN, and PAA (panels A, B, and C). The height of the temperature inversions is very different between the two nights (around 3–4 m for the 8–9th and around 15 m for the 15–16th), resulting in contrasting vertical gradients for the three trace-gases. The height of the temperature inversion remained the same throughout the night, however, the magnitude (*i.e.* the temperature difference between 1 and 28 m) changed. While the relative humidity profiles (panel E) for the 15–16th are similar at the beginning (circles and solid line) and end (triangles and dashed line) of the night, a large change was observed for the 8–9th, which might explain why the change in vertical gradient of O_3, PAN and PAA during the night is different. Temperature inversions and strong gradients in relative humidity such as those observed on the 15–16th can suggest that the atmosphere was very stable, which could lead to a significant reduction in entrainment from above the tree tops. The impact of entrainment, chemical and physical losses on the total observed loss coefficients (*i.e.* lifetimes) of O_3, PAN, and PAA at different heights will be discussed in detail in Sections 3.3–3.5.

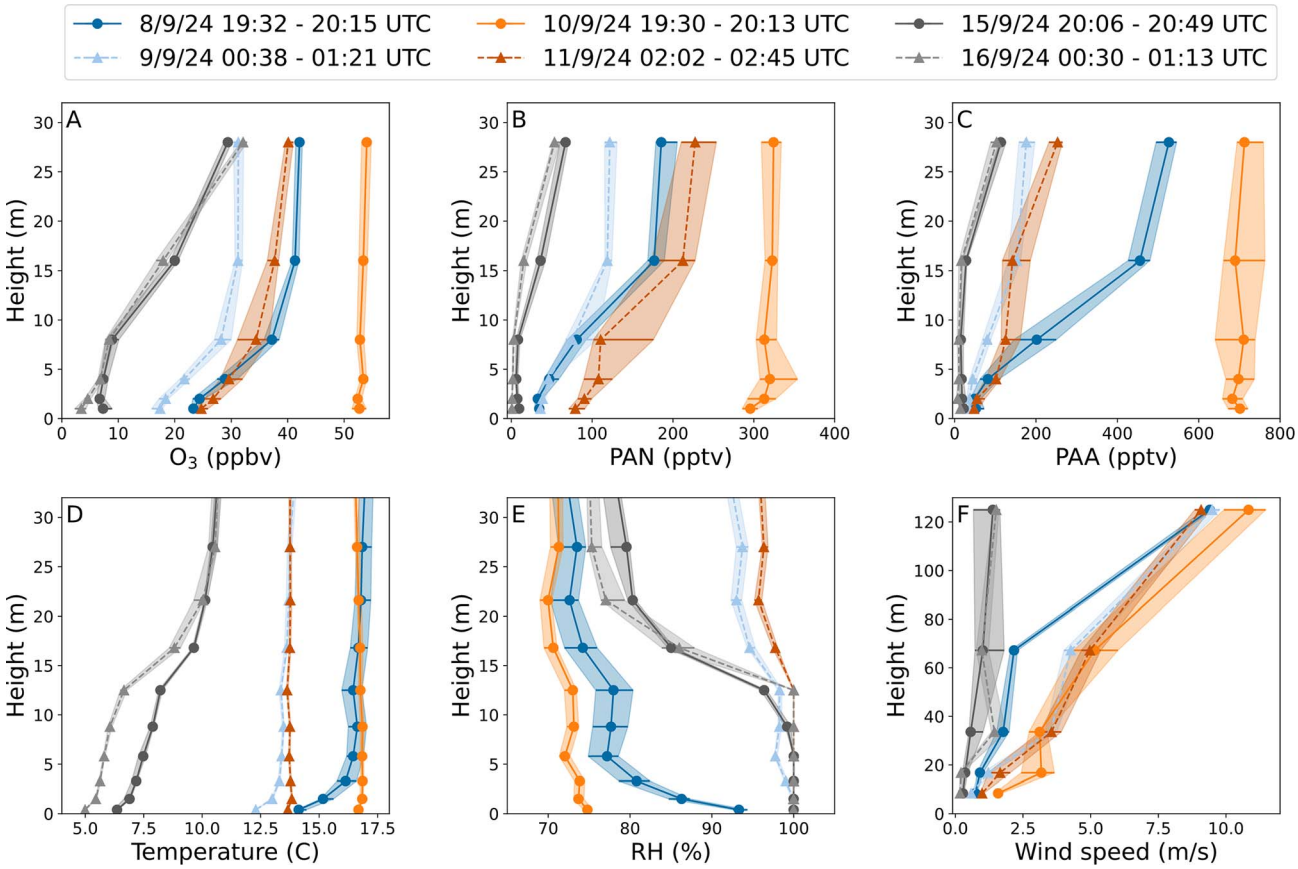

Fig. 2 Examples of individual vertical gradients (each taking ~43 minutes to obtain in which the trace gas inlets were moved from 1 m to 28 m) at the beginning (circles, solid lines) and end (triangles, dashed lines) of three different nights (8/9/24-9/9/24 – blue, 10/9/24–11/9/24 – orange/red, 15/9/24-16/9/24 – grey) of O_3 (A), PAN (B), PAA (C), temperature (D), relative humidity (RH) (E), and wind speed (F). Note that local time is UTC + 3. The circles and triangles show the median at each height during the measurement cycle and the error bars and shading show the 25th and 75th quantile. Note that the height scale for wind speed differs from the other panels to show the significant difference in wind speed above the canopy between different nights.

3.1 Observed loss coefficients (lifetimes) of O_3, PAN, and PAA at nighttime

We define meteorological conditions as stationary during periods when (1) the value of the decoupling constant Ω does not vary more than 0.25 from its median and (2) it does not move between decoupled and coupled conditions (see above). In these periods, the rate of entrainment of air from above the tree tops can be assumed to be constant and the observed (net) loss coefficients of O_3, PAN, and PAA at nighttime can be determined by fitting time dependent mixing ratios at one height to a first-order exponential decay as described in eqn (2):

$$[C]_t = [C]_0 \times e^{(-k_{net} \times t)} \quad (2)$$

where $[C]_0$ and $[C]_t$ are the mixing ratios of O_3, PAN or PAA at time 0 and t, respectively, and k_{net} is the corresponding loss coefficient.

At low levels of solar irradiance PAA is lost predominantly by deposition to surfaces while both O_3 and PAN are additionally removed (thermo)chemically (see below). In this analysis, we consider only measurements, in which the O_3 production from NO_2 photolysis is small compared to the observed O_3 loss (nighttime and in exceptional cases the couple of hours before sunset where the canopy is out of direct sunlight and the sub-canopy is extremely decoupled from above) to avoid the impact of photochemical production or loss. The nighttime production of PAN from NO_3 + isoprene, is considered negligible. We therefore assume that the only source of O_3, PAN and PAA that occurs at nighttime within the canopy is entrainment from air above the tree tops. For O_3 we must also consider reactions with NO (presumably released from the soil (*e.g.* Pilegaard[40])), NO_2 and unsaturated biogenic trace gases emitted by the biosphere. NO emissions from the soil resulted in NO mixing ratios up to 5–20 pptv at 1–4 m and approximately 0 pptv at 8–28 m. For PAN, the major, chemical loss process is its thermal dissociation to NO_2 and the acetyl peroxy radical ($CH_3C(O)O_2$) followed by reactions of $CH_3C(O)O_2$ with NO and other peroxy radicals that prevent the reformation of PAN.

On the night starting on September 9th the pulley system was inoperative and the nights starting on September 13th and 14th were dominated by rain. Loss rate coefficients for O_3, PAN and PAA were therefore derived from data collected on the nights starting on September 7th, 8th, 10th, 11th, and 16–24th

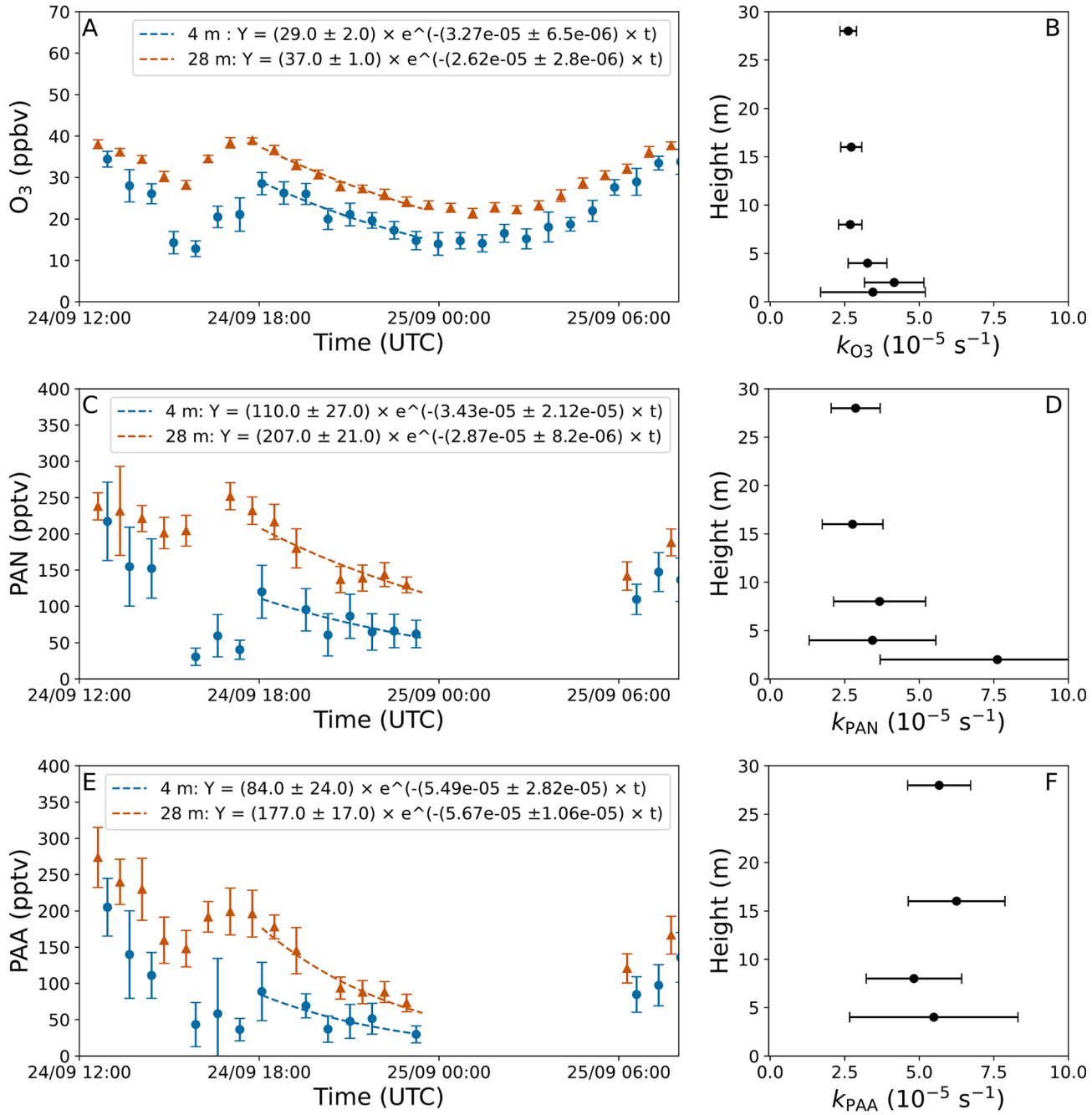

Fig. 3 Panel (A), (C), and (E) show examples of nighttime measurements of O_3, PAN and PAA, respectively, at heights of 4 m (blue circles) and 28 m (red triangles). Each datapoint is the average of one measurement cycle, and the error bars are $\pm 1\sigma$. Local time is UTC + 3. The fits are described by eqn (2) and the resulting loss coefficients for the six measurement heights are plotted in panels (B), (D), and (F), where the error bars are 1σ uncertainties on the fit.

as well as during the evenings of the nights starting on September 12th and 15th, where the majority of the loss took place before sunset, however, the photochemical production of O_3 was low within the sub-canopy ($\leq$1 ppbv h^{-1} based on scaled NO_2 photolysis rates at 5 m and measured NO_2 mixing ratios) and the sub-canopy was extremely decoupled from above (median $\Omega < 0.15$). Measurements of O_3, PAN, and PAA are used in the analysis only if they are significantly different from 0. For O_3 the limit is conservatively set to 2 ppbv. For PAN, data were used when the uncalibrated average PAN + PAA signal exceeded the average PAA signal + 1σ of the PAA signal. For PAA data were used when the average PAA signal exceeded the average background signal + 1σ of the background signal.

Fig. 3 shows exponential fits weighted by the standard deviation (1σ) of the measurements from two different heights for O_3 (A), PAN (C), and PAA (E): the loss coefficients for all six heights measured on this night are plotted against height in panels B, D, and F. The fits to the data began at the highest

mixing ratios observed followed by a decrease in mixing ratios, where Ω remained within the boundaries defined above. The fitted exponentials were only used for further analysis if at least 3 data points were available at each height and the uncertainty (1σ) was less than the fit value of the loss coefficient. The night of September 24–25th was chosen as an example since all three trace gases have good fits for the majority of the heights sampled.

The net loss coefficients obtained throughout the campaign and across all heights were highly variable with values of 0.65–19.0 $\times 10^{-5}$ s^{-1} for O_3 (66 individual values), 0.94–27.1 $\times 10^{-5}$ s^{-1} for PAN (45 individual values) and 1.82–37.6 $\times 10^{-5}$ s^{-1} for PAA (47 individual values), resulting in (net) lifetimes of 1.5–42 h, 1.0–29 h, and 0.7–15 h, respectively. The drivers of the large variability in the net loss terms are discussed in Sections 3.3–3.5. The loss coefficients measured in this study generally agree well with those from other studies conducted in forested regions: previous measurements are summarized in Table 1. Crowley *et al.*[6] determined the loss coefficients for the same trace gases to be 0.93 $\times 10^{-5}$ s^{-1} for O_3, 2.3 $\times 10^{-5}$ s^{-1} for PAN, and 5.2 $\times 10^{-5}$ s^{-1} for PAA for the same site based on average diel profiles. Shepson *et al.*[9] determined the net loss coefficients for O_3 and PAN on a single night to be 2.99 $\times 10^{-5}$ s^{-1} and 8.64 $\times 10^{-5}$ s^{-1}, respectively, in a Canadian mixed deciduous/coniferous forest. And Andersen *et al.*[10] determined the net loss coefficient for O_3 in a French mixed deciduous/coniferous forest to vary from 1.8–30.0 $\times 10^{-5}$ s^{-1} over a month of summertime measurements.

3.2 Relative rate

Shepson *et al.*[9] determined the ratio k_{O_3}/k_{PAN} for the loss of O_3 and PAN in three rural sites in Canada using the "relative rate method", which is well-established for determining rate coefficients in the laboratory. Generally, by plotting the loss of one molecule (reactant) relative to another molecule (reference), the ratio of the rate coefficients $k_{reactant}/k_{reference}$ is obtained as the slope of the plot as shown in eqn (3), where $[reactant]_0$, $[reactant]_t$, $[reference]_0$, and $[reference]_t$ are the concentrations of the reactant and reference at time 0 and t, and $k_{reactant}$ and $k_{reference}$ are the rate coefficients of the reactant and reference, respectively.

$$\ln\left(\frac{[\text{reactant}]_0}{[\text{reactant}]_t}\right) = \frac{k_{\text{reactant}}}{k_{\text{reference}}} \times \ln\left(\frac{[\text{reference}]_0}{[\text{reference}]_t}\right) \quad (3)$$

Here we use the relative rate method to allow us to determine k_{PAN}/k_{O_3} and k_{PAA}/k_{O_3} on nights where the observed loss does not strictly follow exponential behaviour due to less stationary meteorological conditions.

Fig. 4 shows all the relative rate analyses at heights of 1, 2, 4, 8, 16, and 28 m during the BAIRN-VIP campaign for which r^2 was higher than 0.8 and at least 3 datapoints available for the fit. Shepson *et al.*[9] used $r^2 > 0.7$, however, as we do not see a significant reduction in usable fits by using 0.8 (82 and 74 fits

Table 1 Overview of measured nighttime loss coefficients and deposition velocities of O_3 (not exhaustive), PAN, and PAA to relevant surfaces

Location	Surface	Loss coefficient (k_X)	Deposition velocity ($V_d(X)$)	Reference
X = O_3				
Laboratory	Grass		0.47–0.55 cm s^{-1}	Garland and Penkett[41]
Laboratory	Soil		1.6 cm s^{-1}[c]	Garland and Penkett[41]
Laboratory	Alfalfa canopy		1.7 cm s^{-1}	Hill[42]
Dorset, Canada	Deciduous/coniferous forest	2.99 $\times 10^{-5}$ s^{-1}	0.19 cm s^{-1}	Shepson *et al.*[9]
Rambouillet, France	Deciduous/coniferous forest	1.8–30.0 $\times 10^{-5}$ s^{-1}	0.018–0.3 cm s^{-1}[a]	Andersen *et al.*[10]
Hyytiälä, Finland	Coniferous forest		0.05–0.15 cm s^{-1} (winter)	Keronen *et al.*[45]
Hyytiälä, Finland	Coniferous forest	0.93 $\times 10^{-5}$ s^{-1}[b]	0.093 cm s^{-1}[c]	Crowley *et al.*[6]
Hyytiälä, Finland	Coniferous forest	0.65–19.0 $\times 10^{-5}$ s^{-1}	0.11 ± 0.05 cm s^{-1}[d]	This study
Global modelling	Coniferous forest		~0.2 cm s^{-1} (September)	Hardacre *et al.*[46]
X = PAN				
Laboratory	Grass		0.14–0.26 cm s^{-1}	Garland and Penkett[41]
Laboratory	Soil		0.21–0.30 cm s^{-1}[e]	Garland and Penkett[41]
Laboratory	Alfalfa canopy		0.75 cm s^{-1}	Hill[42]
Dorset, Canada	Deciduous/coniferous forest	8.64 $\times 10^{-5}$ s^{-1}	0.54 cm s^{-1}	Shepson *et al.*[9]
Germany	Corn field		0.54 ± 0.94 cm s^{-1}	Schrimpf *et al.*[44]
North Carolina, USA	Loblolly pine plantation		0.2–0.6 cm s^{-1}	Turnipseed *et al.*[12]
California, USA	Ponderosa pine forest		0.05–0.2 cm s^{-1}	Wolfe *et al.*[11]
Hyytiälä, Finland	Coniferous forest	2.3 $\times 10^{-5}$ s^{-1}[b]	0.23 cm s^{-1}	Crowley *et al.*[6]
Hyytiälä, Finland	Coniferous forest	0.94–27.1 $\times 10^{-5}$ s^{-1}	0.15 ± 0.05 cm s^{-1}[d]	This study
X = PAA				
Hyytiälä, Finland	Coniferous forest	5.2 $\times 10^{-5}$ s^{-1}[b]	0.52 cm s^{-1}[c]	Crowley *et al.*[6]
Hyytiälä, Finland	Coniferous forest	1.82–37.6 $\times 10^{-5}$ s^{-1}	0.20 ± 0.11 cm s^{-1}[d]	This study

[a] Assumes no entrainment and a boundary layer height of 20 m. [b] Determined from an average diel profile of the campaign. [c] Calculated assuming the same boundary layer height used for PAN (200 m). [d] Calculated using measurements from two nights, where the sub-canopy was strongly decoupled and a decoupled layer height of 20 m. [e] Increasing values were observed with increasing humidity.

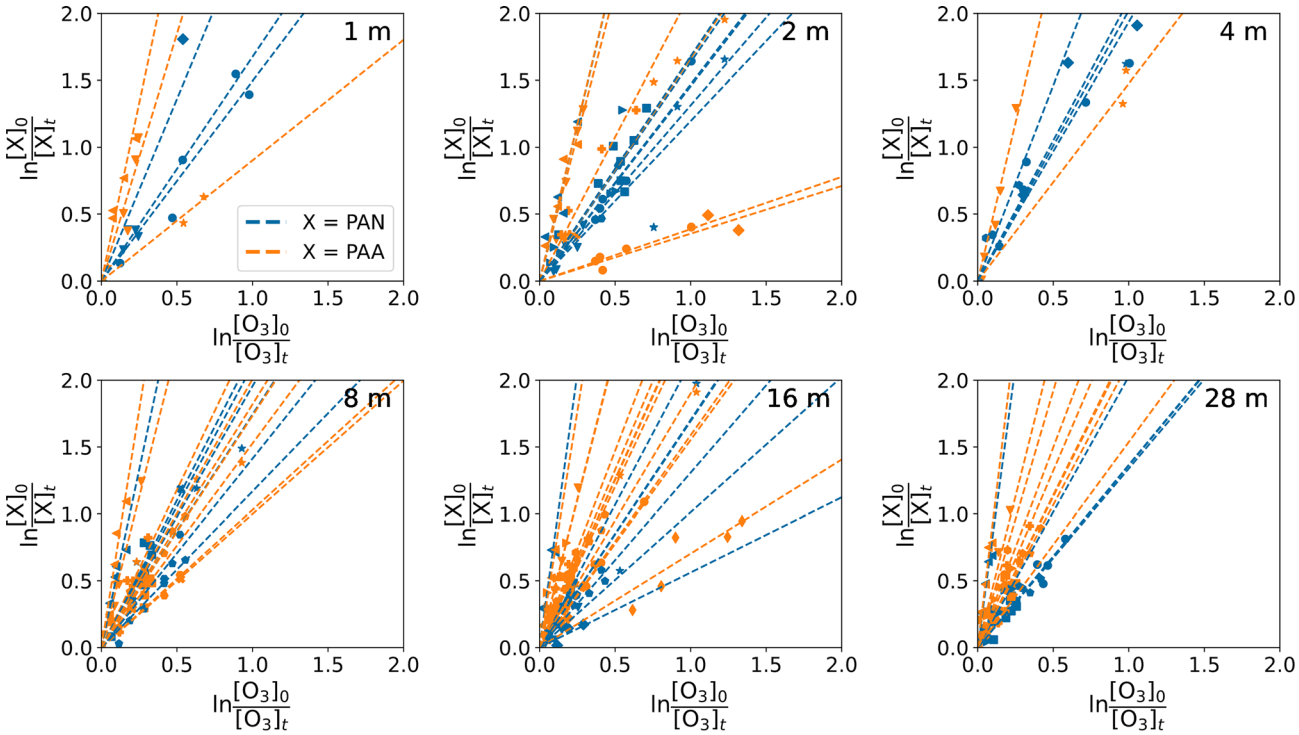

Fig. 4 Relative rates of PAN (blue) or PAA (orange) *versus* O_3 for individual nights at 1, 2, 4, 8, 16, and 28 m during the BAIRN-VIP campaign. Only data where $r^2 > 0.8$ is represented in this figure (see Section 3.2 for more details). A different symbol is used for each night.

when using $r^2 > 0.7$ and $r^2 > 0.8$, respectively) and the slope of plotting the ratios determined using relative rate *versus* the ratios of the rate coefficients determined using first order decays in Section 3.1 (Fig. 5A) is identical whether we use $r^2 > 0.7$ (slope $= 1.01 \pm 0.04$) or $r^2 > 0.8$ (slope $= 1.01 \pm 0.04$), we have chosen 0.8.

There are significantly fewer good fits at 1–4 m (25) compared to 8–28 m (49) (Fig. 4), possibly due to more rapid loss rates near the ground, leaving fewer measurements above the LODs of the instruments. k_{PAN}/k_{O_3} varied from 0.56–8.40 with a median of 1.7 when using the relative rate method, however, the three measurements with ratios above 3 (marked with dashed lines in the frequency distribution in Fig. 5B) are all from the night starting on the 20th of September, where we observed no significant temperature inversion (<0.2 °C between 1.5 and 27 m), a small gradient in O_3 mixing ratios (3–7 ppbv during the fit), and high friction velocities (>0.3 m s^{-1}) at 27 m compared to other nights. This meteorological situation could have resulted in O_3 (but not PAN) being entrained from O_3 rich air above the canopy. The one measurement with a ratio less than 1 has a low starting mixing ratio and very small absolute changes. The remaining ratios are all within the variability of that observed by Shepson *et al.*[9] during three campaigns in Canada ($k_{O_3}/k_{PAN} = 0.42 \pm 0.19$, $k_{PAN}/k_{O_3} = 2.38 \pm 1.08$ (observed variability in k_{PAN}/k_{O_3} = 0.90–4.34)). The ratio previously reported for the Hyytiälä forest station of 2.5 (k_{O_3}/k_{PAN} = 0.4) determined from average diel profiles during the HUMPPA-COPEC campaign is also within our observed variability.[6] Contrary to the field studies which show that PAN is removed faster or at the same rate as O_3 from the atmosphere, laboratory experiments measuring the decrease in O_3 and PAN in a return-flow wind tunnel show the opposite with ratios of 0.13–0.55 for grass and soil,[41] while chamber studies of alfalfa canopy result in a ratio of 0.44.[42] This apparent discrepancy is most likely related to the difference in surface types in a more complex real world environment compared to the simplified laboratory systems.

k_{PAA}/k_{O_3} varied similarly, with ratios ranging from 0.35 to 9.40 with a median of 2.4. The high values above a ratio of 5 (outliers) are also from the night starting on September 20th as shown in the frequency distribution in Fig. 5C. It should be noted that the ratios below 1 are all also determined from nights with low PAA starting mixing ratios at the given height and small absolute changes, which could indicate that the method is not valid for these observations. To our knowledge, this is the first time this ratio has been studied; however, Crowley *et al.*[6] determined loss coefficients for both O_3 and PAA at a height of ~20 m, which would give a ratio of 5.6 for the same site, which is in the high end of our measurements (see Fig. 5A and C), but within the variability. The lower variability observed in the ratio k_{PAN}/k_{O_3} compared to k_{PAA}/k_{O_3} (when excluding the measurements from the 20–21st September) indicates that the surface resistance to uptake of PAN and O_3 has a similar dependence on the same atmospheric variables. In contrast, the controlling factors for PAA, which is a soluble peroxy-acid, are likely to be significantly different and more likely to be influenced by transport rather than by surface resistance to uptake.

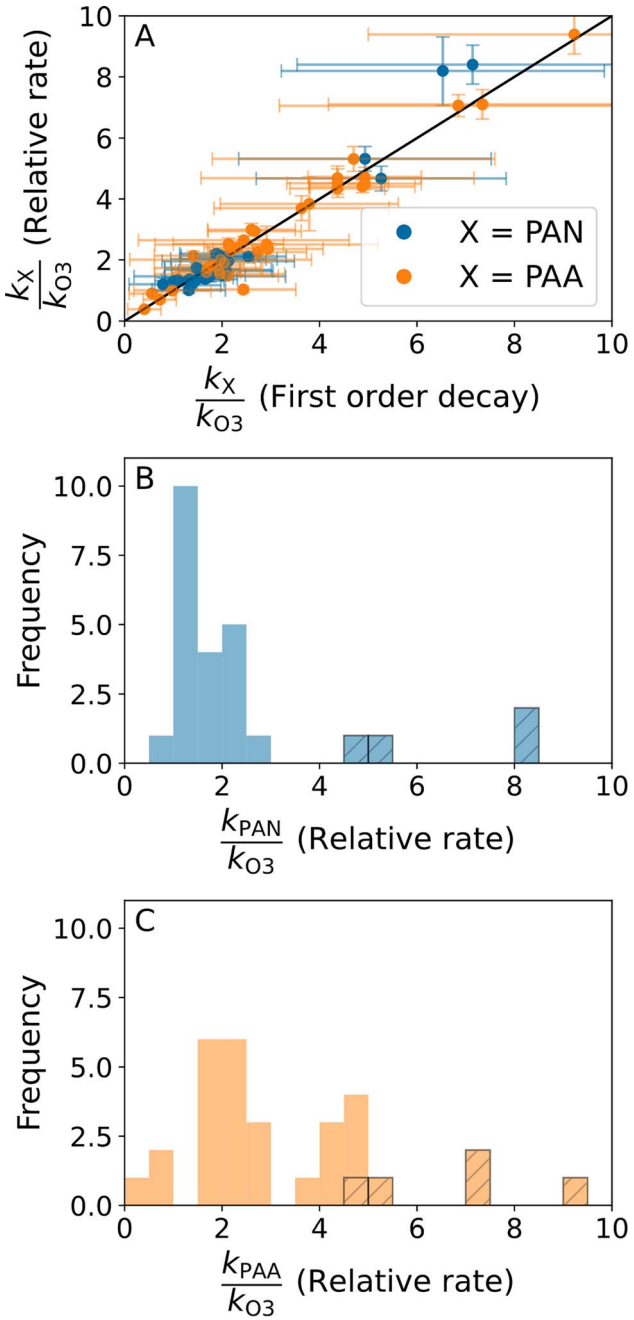

Fig. 5 Panel (A) shows the ratios k_{PAN}/k_{O_3} and k_{PAA}/k_{O_3} determined using the relative rate method plotted against the ratios determined from the first order decays. The uncertainties are the 1σ standard deviation on the fits. The solid, black line is the 1 : 1 ratio. Panel (B) and (C) show the frequency distributions of the ratios k_{PAN}/k_{O_3} and k_{PAA}/k_{O_3} determined using the relative rate method. The dashed areas represent the ratios obtained on the night of the 20–21st of September.

3.3 Physical losses

The sum of physical and chemical loss coefficients can be derived from data obtained on nights when the rate of entrainment is negligible, which occurs when the sub-canopy is completely decoupled from the air above the tree tops. In Fig. 6 we plot the net loss coefficients for O_3 (A), PAN (B), and PAA (C) from Section 3.1 against the median decoupling constant Ω across the fitting period. As is expected, the loss coefficients determined at 28 m (above the tree-tops) show little variation with Ω. When the median $\Omega > 0.43$ the loss coefficients at 1–16 m show a weak variability for all values of Ω and all heights which is a result of deep entrainment. However, when $\Omega < 0.43$ much greater variability is observed. During the period on the 12th and 15th of September over which net losses were measured (orange and blue) Ω was extremely low with a median of 0.075 and 0.12, respectively, indicating that the measurements at 1–16 m are almost completely decoupled from above. The effect of the extreme decoupling is illustrated with the measurements from September 15–16th shown in Fig. 7. On this night, there was an exceptionally strong temperature inversion (shown in Fig. 7A), coincident with a large decrease in Ω (Fig. 7A). The combination of these two phenomena indicates both a high buoyancy force opposing the vertical downward movement of air and the lack of wind-shear turbulence, thereby preventing a coupling of the sub-canopy with the rest of the surface layer.[17,43]

During development of the inversion (15-18 UTC, 18-21 local time (LT)) significant loss of O_3, PAN and PAA was observed, which can be understood in terms of reduction in above-canopy coupling/entrainment leading to large net loss coefficients at the lower heights (*e.g.* 1 and 8 m in Fig. 7B–D). The net loss coefficients at different heights for this time period are plotted in orange in Fig. 6. Once the temperature inversion and Ω have stabilized (18-04 UTC, 21-07 LT) only very weak further losses of O_3, PAN and PAA were observed below the height of the inversion and none above it, which is related to the very low wind speeds throughout the profile (see Fig. 2F).

Based on these observations, we assume that the rate of entrainment is negligible on September 12th and 15th and equate the measured loss coefficient to a combination of physical and chemical losses only. By subtracting the chemical losses for O_3 and PAN (estimated in Section 3.4) and taking an average of the thus derived physical loss coefficients at 1–16 m for these two days we get $(1.1 \pm 0.5) \times 10^{-4}$ s^{-1} for O_3, $(1.5 \pm 0.5) \times 10^{-4}$ s^{-1} for PAN, and $(2.0 \pm 1.1) \times 10^{-4}$ s^{-1} for PAA. Losses of PAA through uptake to aerosols are expected to be negligible in this environment (very low aerosol surface area density) as shown by Crowley *et al.*[6] Loss of PAN and O_3 to aerosol is expected to be even slower. Combining the average physical loss coefficients with a decoupled layer height of 20 m (tree top height), which is reasonable since the measurements below the tree tops are clearly decoupled from above, results in deposition velocities of 0.11 ± 0.05 cm s^{-1}, 0.14 ± 0.05 cm s^{-1}, and 0.20 ± 0.11 cm s^{-1} for O_3, PAN and PAA, respectively. These values are all in reasonable agreement with reported deposition velocities for these trace gases in similar, forested regions (see Table 1 for references). Using flux measurements Wolfe *et al.*[11] and Turnipseed *et al.*[12] determined nocturnal PAN deposition velocities to pine forests of 0.05–0.2 and 0.2–0.6 cm s^{-1}, respectively, while Shepson *et al.*,[9] Schrimpf[44] *et al.* and Crowley *et al.*[6] estimated values of 0.23–0.54 cm s^{-1} to different forests and a corn field using indirect techniques. Similar values were obtained for soil (0.21–0.30 cm s^{-1}) and grass (0.14–0.26 cm s^{-1}) in

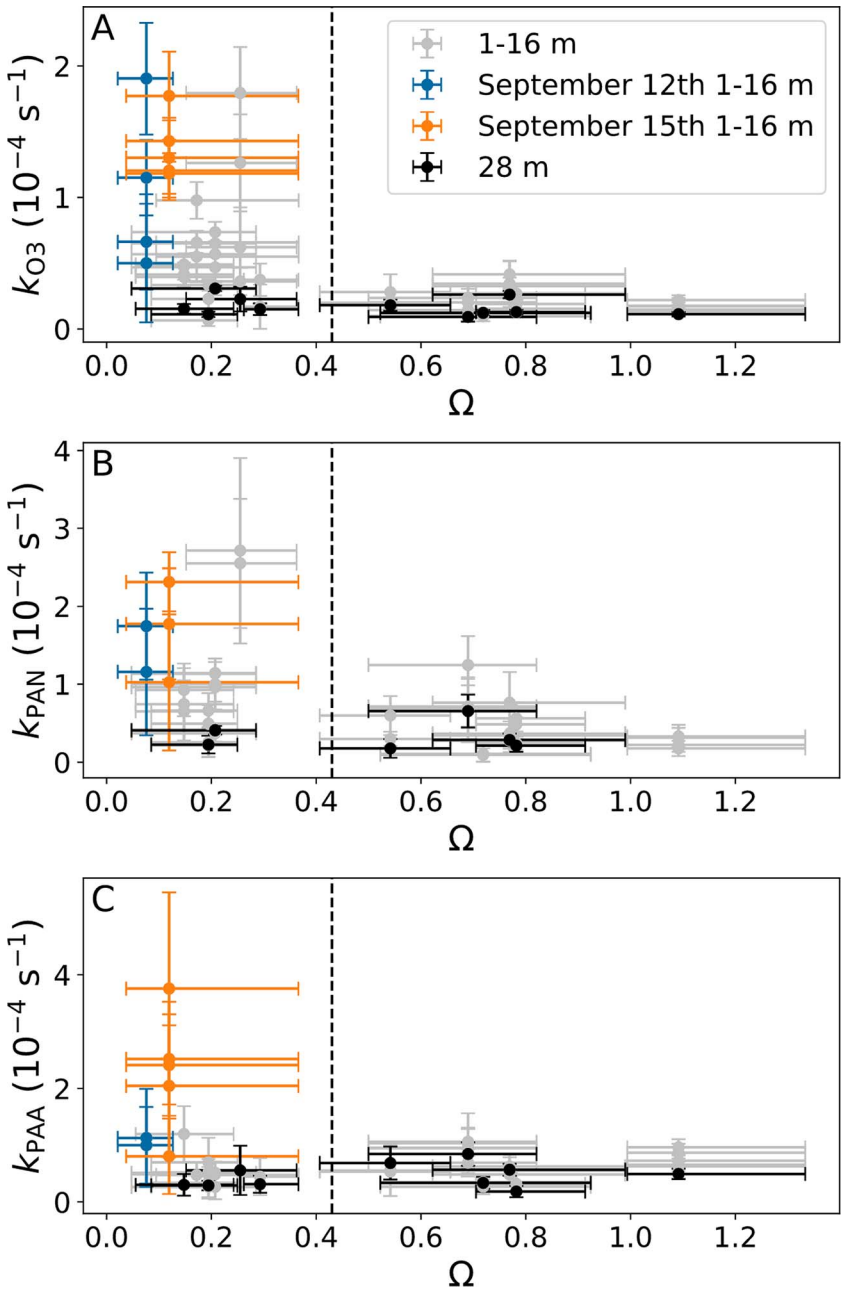

Fig. 6 Net loss coefficients for O_3 (A), PAN (B), and PAA (C) plotted against Ω. Datapoints to the left of the dashed line are clearly decoupled.

laboratory experiments by Garland and Penkett.[41] For PAA we convert the net loss rate determined by Crowley *et al.*[6] into a deposition velocity of 0.52 cm s^{-1} using a mixing layer height of 200 m based on the equation described by Shepson *et al.*,[9] which is a factor 2–3 higher than that estimated here. O_3 deposition velocities have previously been determined at the SMEAR II site for summertime (0.6–0.7 cm s^{-1}) and wintertime (0.05–0.15 cm s^{-1}) by Keronen *et al.*[45] While the summertime values are in good agreement with that determined for grass (0.47–0.55 cm s^{-1}) in a laboratory study, the wintertime values are similar to the value determined in this study and the values determined by Shepson *et al.*,[9] Crowley *et al.*,[6] and Andersen *et al.*[10] of 0.018–0.3 cm s^{-1} for three different forest sites by converting net loss coefficients into deposition velocities and consistent with the deposition velocity used for coniferous forests in September in 15 different global models (around 0.2 cm s^{-1}).[46]

The increase in the physical loss coefficients going from O_3 to PAN to PAA is consistent with the trend in Henry's law solubility constants (~1×10^{-4}, ~2.8×10^{-2} and ~2.5–10 mol m^{-3} Pa^{-1}) compiled by Sander.[47] The rate of deposition of O_3 has previously been observed to be dependent on relative humidity with significantly higher losses and variability when the relative humidity is >70%.[10,25,26] In Fig. S7 we plot the net loss coefficient (corrected for chemical losses) *versus* relative humidity (RH). For PAA we use the total loss coefficients from

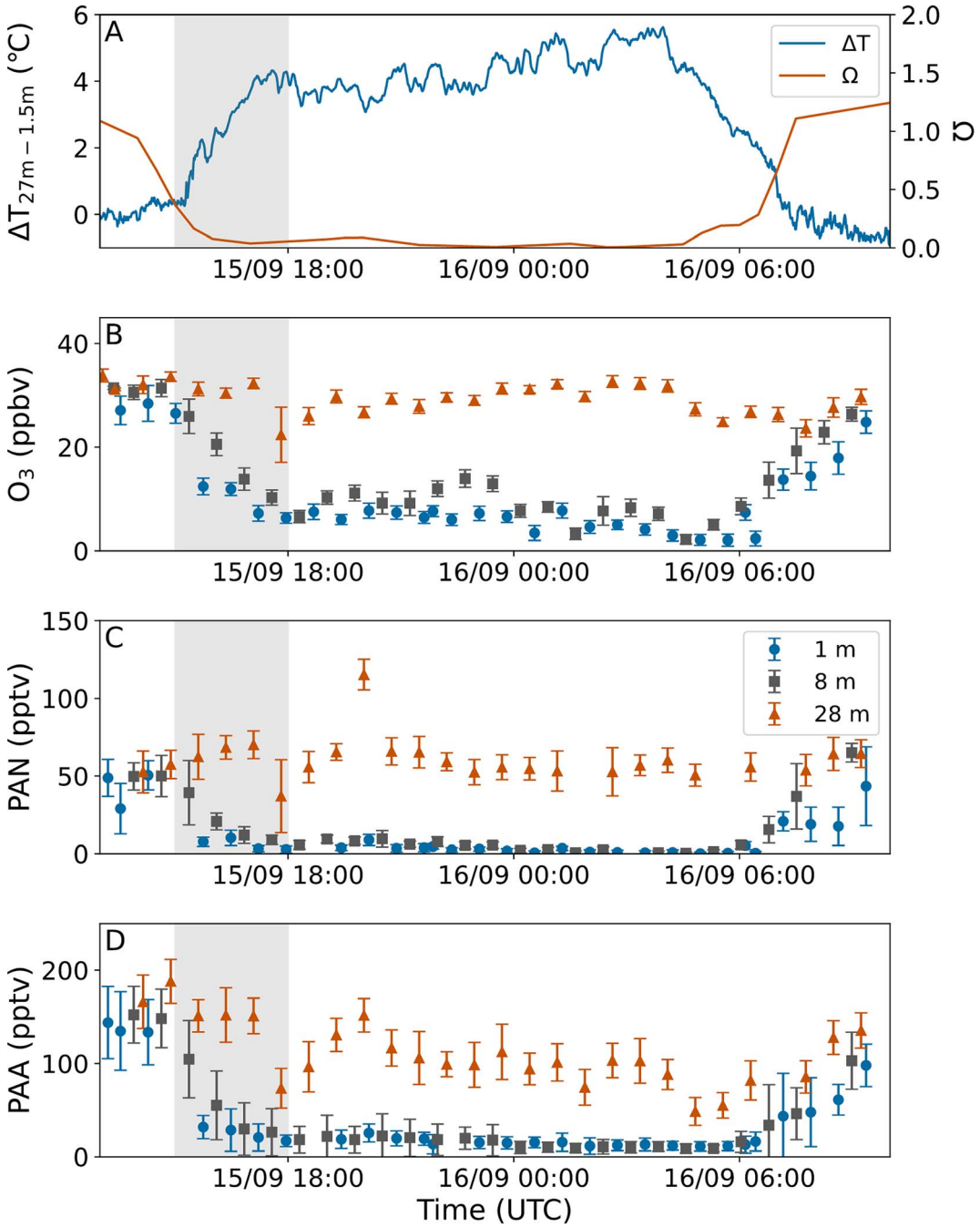

Fig. 7 Time series of ΔT_{27m-1m} and Ω (A), and O_3 (B), PAN (C), and PAA (D) at three different heights, where 28 m is above the temperature inversion and 1 and 8 m are both below. The grey shaded area shows the time period used to determine the deposition coefficients.

Section 3.1; for PAN and O_3 the chemical losses estimated in Section 3.4 have been subtracted from the overall loss rate. No obvious trend is observed for any of the trace gases when taking all data into account, however, O_3 and PAN have the largest loss coefficients and variability at 100% RH like the previous studies when excluding data from the 12th and 15th of September, where the sub-canopy is extremely decoupled from above. For PAA no obvious trend is observed whether the 12th and 15th are included or not, which could be explained if the surface resistance is insignificant compared to the transport resistance. This is because PAA is much more soluble than either O_3 or PAN. The lack of very clear trends for any of the trace gases may be due the restricted range in RH, which was always >70%, and due to the variation in entrainment from night to night. The lack of an RH dependence for PAA, but an observable one for O_3 may partially explain the large variability observed for k_{PAA}/k_{O_3}. In a similar vein, the lower variability in k_{PAN}/k_{O_3} is due to the similar behaviour of the two gases regarding surface resistance to uptake.

The highest net loss coefficients are observed close to the ground; however, the data does not allow us to distinguish between deposition to soil and vegetation. However, previous

measurements have shown that up to 80% of O_3 deposited to a mixed oak-hornbeam forest was removed by the canopy and only 2% by the understory vegetation and soil.[48]

3.4 Nocturnal chemical losses

3.4.1 O_3. The nighttime loss of O_3 due to chemical reactions is dependent on the availability of NO, NO_2 and biogenic volatile organic compounds (BVOCs). O_3 reacts with NO to give NO_2 (R7), NO_2 to give NO_3 (R8) and with BVOCs to form a large variety of oxidized organic compounds (R9).

$$NO + O_3 \rightarrow NO_2 + O_2 \quad (R7)$$

$$NO_2 + O_3 \rightarrow NO_3 + O_2 \quad (R8)$$

$$O_3 + BVOCs \rightarrow products \quad (R9)$$

Using the temperature dependent rate coefficients for reactions (R7) and (R8) (ref. 49) and the height-dependent median temperature, NO and NO_2 mixing ratios for each night, the height-dependent loss of O_3 due to NO_x ((R7) and (R8)) is calculated and plotted in Fig. 8A. Reactions of O_3 with NO and NO_2 contribute around 1–11% of the total O_3 loss rates at 1–2 m with a median around 2–4% (predominantly caused by NO) when assuming the O_3 physical loss coefficient is constant at 1.1×10^{-4} s^{-1}. At 4–28 m, this is reduced to <5% and is almost entirely due to NO_2 when above 8 m.

Height-dependent measurements of BVOCs with which to assess the loss of O_3 *via* (R9) were not available during the campaign. However, the sum of monoterpenes ($\sum$MT) was measured at ~36 m throughout the campaign, speciated MTs were measured *via* GC at 36 m for a short period (two days separated into four-hour periods from September 10–12th) and the height-dependent NO_3 reactivity towards BVOCs was measured throughout. The total NO_3 reactivity towards BVOCs at 28 m when above the LOD is plotted against the $\sum$MT concentration in Fig. S8. We only plot data between 09:00 and 17:00 UTC (local time is UTC + 3) to reduce the impact of vertical gradients between the measurements conducted at 28 and 36 m. Orthogonal distance regression weighted by the uncertainty in the NO_3 reactivity gives a slope of 5.60×10^{-12} cm^3 $molecule^{-1}$ s^{-1} with a 3σ uncertainty of 0.5×10^{-12} cm^3 $molecule^{-1}$ s^{-1}, which is similar to the recommended rate coefficient for α-pinene with NO_3 at 298 K.[49] It is, however, important to note that large variations in the monoterpene speciation have been observed at this time of year at this site,[50] we therefore expand the uncertainty to 1.0×10^{-12} cm^3 $molecule^{-1}$ s^{-1}.

The speciation of monoterpenes measured on September 10–12th is shown in Fig. S9. Only four monoterpenes were measured above the limit of detection (α-pinene, camphene, β-pinene, and Δ-carene), which on average accounted for 75% (64–93%) of the measured $\sum$MT by the PTR. The average contribution to the $\sum$MT measured by the GC-MS for the four monoterpenes was 55% α-pinene, 14% camphene, 11% β-pinene, and 20% Δ-carene. This composition of monoterpenes results in an average rate coefficient with NO_3 of 5.60×10^{-12} cm^3 $molecule^{-1}$ s^{-1}, which is identical with that estimated from the measured $\sum$MT by the PTR and the NO_3 reactivity throughout the campaign and similar with that determined from speciated MT measurements of 6.3×10^{-12} cm^3 $molecule^{-1}$ s^{-1} for a different year.[51] The same relative MT composition results in an average rate coefficient of 6.48×10^{-17} cm^3 $molecule^{-1}$ s^{-1} for reactions with O_3. In order to calculate the height-dependent contribution of O_3 loss *via* its reactions with monoterpenes we scale the NO_3 reactivity by $k_{O_3+MT}/k_{NO_3+MT} = 1.15 \times 10^{-5}$ determined from the speciated measurements at 36 m. The uncertainty in the scaling factor is determined as the variation in the ratio for the individual monoterpenes measured ($0.08–1.54 \times 10^{-5}$). In summary, this analysis, while not direct, allows us to calculate a height-dependent mixing ratio for the MTs observed at 36 m which we can use to derive the O_3 reactivity towards the same MTs (see below).

In Fig. 8B we have multiplied the measured median NO_3 reactivity for each night at each height with $k_{O_3+MT}/k_{NO_3+MT} = 1.15 \times 10^{-5}$ to give the average loss rate coefficient of O_3 that can be attributed to monoterpenes and used the extremes ($0.08–1.54 \times 10^{-5}$) to define the error bars. This results in median contributions from monoterpenes of <1% of the total O_3 loss due to physical and chemical loss processes for the campaign across the gradient.

O_3 also react with sesquiterpenes for which the rate coefficients are large with *e.g.* a value of 1.2×10^{-14} cm^3 $molecule^{-1}$ s^{-1} for β-caryophyllene at 298 K (ref. 49) which is the dominant sesquiterpene at this site.[51] No sesquiterpenes were measured during the campaign, so we use the ratios in concentration between β-caryophyllene and α-pinene, β-pinene, and Δ-carene (0.061 ± 0.002, 0.294 ± 0.011, and 0.181 ± 0.007, respectively) for the same site at the same time of year[50] to calculate a median mixing ratio of β-caryophyllene at 36 m for the campaign of 6.0 ± 0.5 pptv with 25th and 75th percentiles of 4.1 ± 0.3 pptv and 9.5 ± 0.5 pptv. This value is in good agreement with previous measurements of sesquiterpenes for the same site and time of year.[51] The sesquiterpene (β-caryophyllene) concentration is then estimated at each height using the height dependent MT mixing ratios (see above), the α-pinene fraction and the ratio to α-pinene determined in Liebmann *et al.*[50] resulting in median mixing ratios between 6 pptv at 28 m and 14 pptv at 1 m for the nights analysed in this study. While β-caryophyllene also reacts rapidly with NO_3 and would therefore contribute to the measured NO_3 reactivity, the estimated mixing ratios only result in a median reactivity of around 0.006 s^{-1}, which is below the average LOD of the measurements. In addition, β-caryophyllene would be transmitted inefficiently through the sampling line of the NO_3-reactivity instrument.

Using the recommended rate coefficient for O_3 + β-caryophyllene and the estimated β-caryophyllene concentration at each height results in a median contribution to the total O_3 loss throughout the gradient of approximately 2–5% (see Fig. 8B). It should be noted that this estimate is associated with high uncertainties due to the lack of any sesquiterpene measurements. The combined median chemical losses of O_3 (all the black triangles in Fig. 8A and B added together) account for 2–

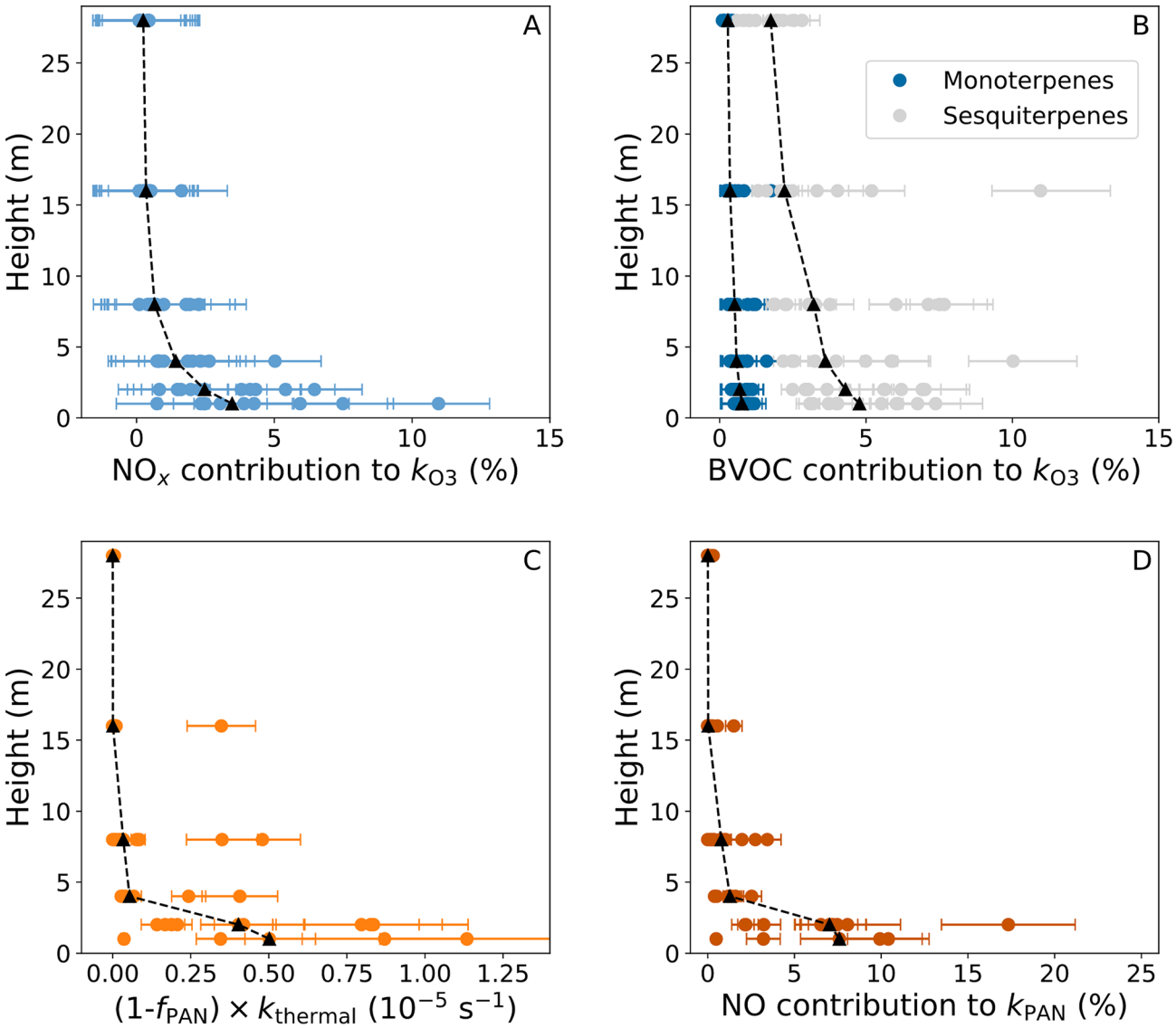

Fig. 8 Panel (A) shows the contribution of NO_x (circles) to the total loss of O_3 at each height. The error bars represent the uncertainty in the NO and NO_2 measurements (it does not include the systematic uncertainty in the rate coefficients or the uncertainty of the fit of the O_3 loss coefficient). Panel (B) shows the contribution from monoterpenes (blue circles) and sesquiterpenes (grey circles) to the total loss of O_3. The error bars for the monoterpene and sesquiterpene reactions include uncertainty in the calculated mixing ratios (see text for details). Panel (C) displays the effective thermal decomposition coefficient of PAN at each height considering reaction of $CH_3C(O)O_2$ with NO and NO_2. The error bars represent the uncertainty in f_{PAN} and 10% on the thermal decomposition coefficient. Panel (D) shows the NO contribution to the total loss of PAN at each height. The error bars represent the uncertainty in the effective thermal decomposition coefficient (see text for details). The black triangles plotted in all panels show the median for each height and the dashed lines serve to highlight the trend.

9% of the net O_3 loss, with chemical losses being most important close to the ground. Physical losses (*i.e.* deposition) therefore account for > 90% of the O_3 loss when set to a constant value of 1.1×10^{-4} s^{-1} determined from two evenings, where entrainment is assumed to be very small.

3.4.2 PAN. As PAN itself does not react rapidly with oxidants such as OH or O_3, its chemical losses occur subsequent to its thermal decomposition to the acetyl peroxy radical ($CH_3C(O)O_2$, (R1)). $CH_3C(O)O_2$ can react with NO_2 to reform PAN (R10) in a sequence that does not lead to the net loss of PAN or react with NO, hydroperoxyl radicals (HO_2), or other peroxy radicals (RO_2) to irreversibly remove PAN from the atmosphere ((R11)–(R13)).

$$CH_3C(O)OONO_2 + M \rightarrow CH_3C(O)O_2 + NO_2 + M \quad (R1)$$

$$CH_3C(O)O_2 + NO_2 + M \rightarrow CH_3C(O)OONO_2\ (PAN) + M \quad (R10)$$

$$CH_3C(O)O_2 + NO \rightarrow CH_3O_2 + NO_2 + CO_2 \quad (R11)$$

$$CH_3C(O)O_2 + HO_2 \rightarrow CH_3C(O)OOH\ (PAA) + O_2 \quad (R12a)$$

$$\rightarrow CH_3O_2 + OH + CO_2 \quad (R12b)$$

$$\rightarrow CH_3C(O)OH + O_3 \quad \text{(R12c)}$$

$$CH_3C(O)O_2 + RO_2 \rightarrow \text{products} \quad \text{(R13)}$$

The fraction of $CH_3C(O)O_2$ radicals that reforms PAN (f_{PAN}) through reaction (R10) can be calculated using eqn (4), where k_X is the rate coefficient for reaction (RX)[49] and [Y] is the mixing ratio of compound Y. During BAIRN-VIP there were no peroxy radical measurements and we therefore calculate an upper limit of the reformation of PAN by only taking the reaction with NO (R11) into account (eqn (5)).

$$f_{PAN} = \frac{k_{10}[NO_2]}{k_{10}[NO_2] + k_{11}[NO] + k_{12}[HO_2] + k_{13}[RO_2]} \quad (4)$$

$$f_{PAN} < \frac{k_{10}[NO_2]}{k_{10}[NO_2] + k_{11}[NO]} \quad (5)$$

By multiplying $(1 - f_{PAN})$ with the thermal decomposition rate of PAN at each height, we calculate the lower limit of the effective thermal (chemical) loss coefficient of PAN, which is plotted against height in Fig. 8C. Here we see an increase in the effective thermal loss coefficient with decreasing height due to the accompanying increase in NO. The contribution of the reaction with NO towards the total PAN loss is estimated using a physical loss coefficient of 1.5×10^{-4} s^{-1} determined in Section 3.3 and plotted as a function of height in Fig. 8D. It can be observed to follow the same trend as the O_3 loss due to NO with the lowest median fractions at 4–28 m (0–2%) and the highest fractions at 1–2 m (7–8%), which is closest to the source of the NO (the soil).

While there were no peroxy radical measurements during BAIRN-VIP there were measurements of HO_2 during the HUMPPA-COPEC campaign at the Hyytiälä forest site[52] and modelling of RO_2,[6] resulting in a combined XO_2 ($HO_2 + RO_2$) of around 6×10^8 molecule cm^{-3} (~25 pptv) at nighttime. With similar rate coefficients for reaction (R11)–(R13) of around 2×10^{-11} cm^3 molecule^{-1} s^{-1} at 298 K (ref. 49) we would expect similar contributions to the chemical loss of PAN from XO_2 as we calculate close to the ground for NO if we assumed the same mixing ratio of XO_2 as that modelled during HUMPPA-COMPEC. However, RO_2 and HO_2 are both produced from ozonolysis at nighttime, and while the average diel profile of O_3 for HUMPPA-COPEC reached a minimum of approximately 35 ppbv at ~20 m,[6] the nighttime average across the BAIRN-VIP campaign at 16 m was only around 24 ppbv. The lower O_3 mixing ratios combined with the lower temperatures (and thereby likely lower BVOC mixing ratios) would result in significantly lower HO_2 and RO_2 mixing ratios during BAIRN-VIP than during HUMPPA-COPEC. It is therefore reasonable to assume that the chemical loss of PAN due to reactions of $CH_3C(O)O_2$ with HO_2 and RO_2 at nighttime was small.

3.5 Entrainment

The vertical mixing of air within the stable nighttime boundary layer (entrainment) is controlled by the friction velocity which is related to the horizontal wind speed.[16–20] The entrainment rate coefficient (k_{ent}) is the same for all trace gases, however, the rate of entrainment is also dependent on the mixing ratio of the trace gas above the tree tops. Here we estimate the entrainment rate coefficient by rearranging eqn (1) into (6):

$$k_{ent_h} = \left(k_{net_h} + k_{phys_h} + k_{chem_h}\right) \frac{[C]_h}{[C]_{above}} \quad (6)$$

where k_{enth}, k_{neth}, k_{physh}, and k_{chemh} are the first-order rate coefficients (in s^{-1}) for entrainment, net loss, physical loss, and chemical loss for height h, respectively. Note that k_{neth} is the same as $\frac{d[C]}{dt[C]_h}$ in eqn (1). $[C]_h$ and $[C]_{above}$ are the mixing ratios of trace gas C at height h and at heights above the canopy, respectively. In Fig. 9 we plot estimated entrainment coefficients for PAN (panel A) and PAA (panel B) against those for O_3 when assuming k_{physh} is constant throughout the campaign at the values determined in Section 3.3. Negative entrainment coefficients are obtained when k_{neth} is larger than the average physical loss coefficient determined in this study. In both cases

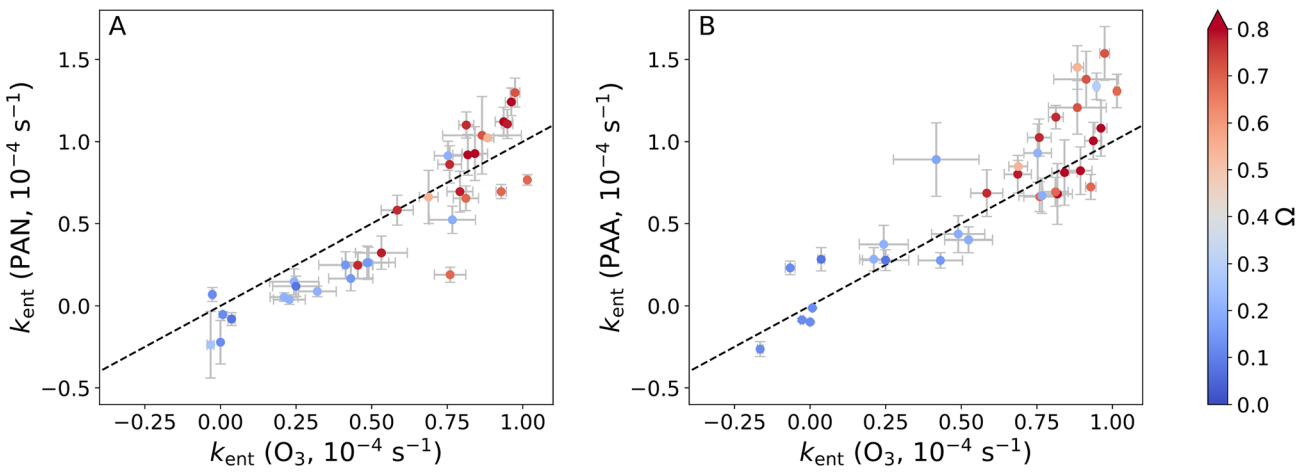

Fig. 9 Estimated entrainment coefficients for PAN (A) and PAA (B) plotted against the estimated entrainment coefficients for O_3 coloured by Ω. The error bars symbolise the variability (1σ) on the estimated k_{ent} during the fitting period. The black dashed lines show the 1 : 1 relationship.

the entrainment coefficients from different heights and nights scatter around the 1 : 1 line showing that, as expected, the same entrainment coefficient is required for all three trace gases. The deviation from the 1 : 1 line can readily be explained by the uncertainties in the trace gas measurements, the fits resulting in the rate coefficients, and the assumption that the physical loss coefficient is constant across different conditions. However, the large variability observed in the required entrainment coefficients is much greater than the observed deviations from the 1 : 1 line showing that entrainment and therefore atmospheric stability have a significant impact on the observed nocturnal trace gas gradients as well as the observed net losses at different heights, which is in agreement with observations for O_3 by Zha *et al.*[21] It is therefore also clear that the entrainment source term is generally not negligible compared to the observed net loss terms (*e.g.* entrainment coefficients on coupled nights are around $\sim 1 \times 10^{-4}$ s^{-1} for all three trace gases, which is similar to the physical loss coefficients). Neglection of the vertical transport would therefore lead to biased estimates of the sum of the physical and chemical losses.

4 Summary and conclusions

This study used measurements of O_3, PAN and PAA at 6 different heights at the SMEAR II site in a boreal forest to investigate the role of chemical and physical loss processes as well as entrainment in defining the lifetimes and vertical gradients of these trace gases. Absolute (net) loss coefficients were determined to vary between 0.65–19.0 $\times 10^{-5}$ s^{-1} for O_3, 0.94–27.1 $\times 10^{-5}$ s^{-1} for PAN, and 1.82–37.6 $\times 10^{-5}$ s^{-1} for PAA, resulting in (net) lifetimes of 1.5–42 h, 1.0–29 h, and 0.7–15 h, respectively, across all heights and throughout the campaign. These observations are consistent with previous measurements of lifetimes for O_3, PAN, and PAA in forested regions. Relative rate determinations of k_{PAN}/k_{O_3} and k_{PAA}/k_{O_3} were made at all heights. k_{PAN}/k_{O_3} and k_{PAA}/k_{O_3} varied between 0.56–8.40 and 0.35–9.40, respectively, with medians of 1.7 and 2.4. The value for k_{PAN}/k_{O_3} is consistent with those reported by Shepson *et al.*[9]

Entrainment of above-canopy air has a major impact on the observed gradients in O_3, PAN, and PAA. On nights where the sub-canopy is coupled with above ($\Omega > 0.43$) the entrainment rate coefficient is $\sim 1 \times 10^{-4}$ s^{-1} for all three trace gases, which is similar to the physical loss coefficients (see below).

Assignment of the contributing loss terms for each trace gas was possible during nights when the sub-canopy was strongly decoupled ($\Omega < 0.43$) from above resulting in a significantly reduced (negligible) rate of entrainment. During BAIRN-VIP, two nights were extremely decoupled with a median $\Omega < 0.15$. By assuming that entrainment was negligible on these nights and subtracting losses due to chemistry, physical loss coefficients were estimated to be $(1.1 \pm 0.5) \times 10^{-4}$ s^{-1} for O_3, $(1.5 \pm 0.5) \times 10^{-4}$ s^{-1} for PAN, and $(2.0 \pm 1.1) \times 10^{-4}$ s^{-1} for PAA resulting in deposition velocities of 0.11 ± 0.05 cm s^{-1}, 0.14 ± 0.05 cm s^{-1}, and 0.20 ± 0.11 cm s^{-1}, when using a decoupled layer height of 20 m (tree top height).

Reactions of O_3 with NO, NO_2 and BVOCs result in an estimated median fraction of 2–9% of the total O_3 loss being due to gas phase chemistry, with the highest values obtained close to the ground, where reaction with NO is most important. Chemical losses of PAN contribute 0–8% of the total loss, with the highest values closest to the ground, owing to the presence of NO. The remaining >90% of the O_3 and PAN loss are attributed to physical losses, while 100% of the PAA loss is due to physical losses.

Author contributions

Conceptualization: STA, JNC, TP, ME. Methodology: STA, JNC. Formal analysis: STA, PD. Investigation: STA, CN, LW, PD, GNTET, JS, IY, LRA, RR, HB, TM, JNC. Resources: HF, ME, TP, JL, JNC. Writing – original draft: STA and JNC. Writing – review and editing: STA, CN, LW, PD, GNTET, JS, HF, ME, TP, ÜR, IY, LRA, RR, HB, TM, JL, JNC. Visualization: STA. Project administration: JNC. Funding acquisition: JNC, TP.

Conflicts of interest

The authors declare that they have no conflict of interest.

Data availability

Continuous meteorology measurements from the mast is accessible through the Fairdata services.[53] Measurements of O_3, PAN, PAA, NO_x, NO_3 reactivity, and the sum of monoterpenes are uploaded to Edmond (https://doi.org/10.17617/3.PBGFBI). Speciated monoterpene data is in Table S1 in the Supplementary information (SI). Supplementary information: time series at different heights of trace gases and meterological parameters as well as information on the monoterpenes measured during the campaign. See DOI: https://doi.org/10.1039/d5ea00159e.

Acknowledgements

STA is thankful to the Alexander von Humboldt foundation for funding her stay at MPIC. PD gratefully acknowledges the Deutsche Forschungsgemeinschaft (project "MONOTONS", project number: 522970430). ME acknowledges the Jane and Aator Erkko Foundation (grant no. 220043). We gratefully acknowledge financial support *via* the ATMO-ACCESS Trans National Access program under ATMO-TNA-3-0000000024 (NORACHO) and ATMO-TNA-7-0000000016 (BAIRN-VIP). All authors thank the SMEAR II station and its staff for help with organizing the campaign and for supporting the people conducting the measurements throughout the campaign, ACTRIS for the monoterpene measurements with Vocus PTR-TOF, and Uwe Parchatka for his help running the O_3 and NO_x measurements. Open Access funding provided by the Max Planck Society.

Notes and references

1 P. J. Crutzen, Photochemical reactions initiated by and influencing ozone in unpolluted tropospheric air, *Tellus*, 1974, **XXVI**, 47–57.
2 R. Atkinson and J. Arey, Gas-phase tropospheric chemistry of biogenic volatile organic compounds: a review, *Atmos. Environ.*, 2003, **37**, S197–S219.
3 H. B. Singh, Reactive nitrogen in the troposphere, *Environ. Sci. Technol.*, 1987, **21**, 320–327.
4 J. M. Roberts, The atmospheric chemistry of organic nitrates, *Atmos. Environ., Part A*, 1990, **24**, 243–287, DOI: 10.1016/0960-1686(90)90108-y.
5 E. V. Fischer, D. J. Jacob, R. M. Yantosca, M. P. Sulprizio, D. B. Millet, J. Mao, F. Paulot, H. B. Singh, A. Roiger, L. Ries, R. W. Talbot, K. Dzepina and S. P. Deolal, Atmospheric peroxyacetyl nitrate (PAN): a global budget and source attribution, *Atmos. Chem. Phys.*, 2014, **14**, 2679–2698, DOI: 10.5194/acp-14-2679-2014.
6 J. N. Crowley, N. Pouvesle, G. J. Phillips, R. Axinte, H. Fischer, T. Petäjä, A. Nölscher, J. Williams, K. Hens, H. Harder, M. Martinez-Harder, A. Novelli, D. Kubistin, B. Bohn and J. Lelieveld, Insights into HOx and ROx chemistry in the boreal forest via measurement of peroxyacetic acid, peroxyacetic nitric anhydride (PAN) and hydrogen peroxide, *Atmos. Chem. Phys.*, 2018, **18**, 13457–13479, DOI: 10.5194/acp-18-13457-2018.
7 G. J. Phillips, N. Pouvesle, J. Thieser, G. Schuster, R. Axinte, H. Fischer, J. Williams, J. Lelieveld and J. N. Crowley, Peroxyacetyl nitrate (PAN) and peroxyacetic acid (PAA) measurements by iodide chemical ionisation mass spectrometry: first analysis of results in the boreal forest and implications for the measurement of PAN fluxes, *Atmos. Chem. Phys.*, 2013, **13**, 1129–1139, DOI: 10.5194/acp-13-1129-2013.
8 X. Zhang, Z. M. Chen, S. Z. He, W. Hua, Y. Zhao and J. L. Li, Peroxyacetic acid in urban and rural atmosphere: concentration, feedback on PAN-NO(x) cycle and implication on radical chemistry, *Atmos. Chem. Phys.*, 2010, **10**, 737–748.
9 P. B. Shepson, J. W. Bottenheim, D. R. Hastie and A. Venkatram, Determination of the relative ozone and PAN deposition velocities at night, *Geophys. Res. Lett.*, 1992, **19**, 1121–1124, DOI: 10.1029/92gl01118.
10 S. T. Andersen, M. R. McGillen, C. Xue, T. Seubert, P. Dewald, G. N. T. E. Türk, J. Schuladen, C. Denjean, J. C. Etienne, O. Garrouste, M. Jamar, S. Harb, M. Cirtog, V. Michoud, M. Cazaunau, A. Bergé, C. Cantrell, S. Dusanter, B. Picquet-Varrault, A. Kukui, A. Mellouki, L. J. Carpenter, J. Lelieveld and J. N. Crowley, Measurement report: Sources, sinks, and lifetime of NOx in a suburban temperate forest at night, *Atmos. Chem. Phys.*, 2024, **24**, 11603–11618, DOI: 10.5194/acp-24-11603-2024.
11 G. M. Wolfe, J. A. Thornton, R. L. N. Yatavelli, M. McKay, A. H. Goldstein, B. LaFranchi, K. E. Min and R. C. Cohen, Eddy covariance fluxes of acyl peroxy nitrates (PAN, PPN and MPAN) above a Ponderosa pine forest, *Atmos. Chem. Phys.*, 2009, **9**, 615–634.
12 A. A. Turnipseed, L. G. Huey, E. Nemitz, R. Stickel, J. Higgs, D. J. Tanner, D. L. Slusher, J. P. Sparks, F. Flocke and A. Guenther, Eddy covariance fluxes of peroxyacetyl nitrates (PANs) and NOy to a coniferous forest, *J. Geophys. Res.: Atmos.*, 2006, **111**, D09304, DOI: 10.1029/2005JD006631.
13 P. Hari and M. Kulmala, Station for Measuring Ecosystem–Atmosphere Relations (SMEAR II), *Boreal Environ. Res.*, 2005, **10**, 315–322, DOI: 10.1007/978-94-007-5603-8_9.
14 I. Neefjes, M. Laapas, Y. Liu, E. Médus, E. Miettunen, L. Ahonen, L. Quéléver, J. Aalto, J. Bäcks, V. M. Kerminen, J. Lampilahti, K. Luomao, M. Mäki, I. Mammarella, T. Petäjä, M. Räty, N. Sarnela, I. Ylivinkka, S. Hakala, M. Kulmala, T. Nieminen and A. Lintunen, 25 years of atmospheric and ecosystem measurements in a boreal forest - Seasonal variation and responses to warm and dry years, *Boreal Environ. Res.*, 2022, **27**, 1–31.
15 X. Chen, L. L. J. Quéléver, P. L. Fung, J. Kesti, M. P. Rissanen, J. Bäck, P. Keronen, H. Junninen, T. Petäjä, V. M. Kerminen and M. Kulmala, Observations of ozone depletion events in a Finnish boreal forest, *Atmos. Chem. Phys.*, 2018, **18**, 49–63, DOI: 10.5194/acp-18-49-2018.
16 B. Schilperoort, M. Coenders-Gerrits, C. Jiménez Rodríguez, C. van der Tol, B. van de Wiel and H. Savenije, Decoupling of a Douglas fir canopy: a look into the subcanopy with continuous vertical temperature profiles, *Biogeosciences*, 2020, **17**, 6423–6439, DOI: 10.5194/bg-17-6423-2020.
17 O. Peltola, T. Aslan, M. Aurela, A. Lohila, I. Mammarella, D. Papale, C. K. Thomas, T. Vesala and T. Laurila, Towards an enhanced metric for detecting vertical flow decoupling in eddy covariance flux observations, *Agric. For. Meteorol.*, 2025, **362**, 110326, DOI: 10.1016/j.agrformet.2024.110326.
18 P. Alekseychik, I. Mammarella, S. Launiainen, Ü. Rannik and T. Vesala, Evolution of the nocturnal decoupled layer in a pine forest canopy, *Agric. For. Meteorol.*, 2013, **174–175**, 15–27, DOI: 10.1016/j.agrformet.2013.01.011.
19 D. D. Baldocchi, Turbulent transfer in a deciduous forest, *Tree Physiol.*, 1989, **5**, 357–377, DOI: 10.1093/treephys/5.3.357.
20 H. Pleijel, G. Wallin, P. E. Karlsson and L. Skärby, Ozone gradients in a spruce forest stand in relation to wind speed and time of the day, *Atmos. Environ.*, 1996, **30**, 4077–4084, DOI: 10.1016/1352-2310(96)00141-0.
21 Q. Zha, C. Yan, H. Junninen, M. Riva, N. Sarnela, J. Aalto, L. Quéléver, S. Schallhart, L. Dada, L. Heikkinen, O. Peräkylä, J. Zou, C. Rose, Y. Wang, I. Mammarella, G. Katul, T. Vesala, D. R. Worsnop, M. Kulmala, T. Petäjä, F. Bianchi and M. Ehn, Vertical characterization of highly oxygenated molecules (HOMs) below and above a boreal forest canopy, *Atmos. Chem. Phys.*, 2018, **18**, 17437–17450, DOI: 10.5194/acp-18-17437-2018.
22 J. H. Seinfeld, *Atmospheric Chemistry and Physics of Air Pollution*, John Wiley and Sons, 1986.
23 E. R. Delaria, B. K. Place, A. X. Liu and R. C. Cohen, Laboratory measurements of stomatal NO2 deposition to

native California trees and the role of forests in the NOx cycle, *Atmos. Chem. Phys.*, 2020, **20**, 14023–14041, DOI: 10.5194/acp-20-14023-2020.

24 D. D. Baldocchi, B. B. Hicks and P. Camara, A canopy stomatal resistance model for gaseous deposition to vegetated surfaces, *Atmos. Environ.*, 1987, **21**, 91–101, DOI: 10.1016/0004-6981(87)90274-5.

25 N. Altimir, P. Kolari, J. P. Tuovinen, T. Vesala, J. Bäck, T. Suni, M. Kulmala and P. Hari, Foliage surface ozone deposition: a role for surface moisture?, *Biogeosciences*, 2006, **3**, 209–228, DOI: 10.5194/bg-3-209-2006.

26 Ü. Rannik, N. Altimir, I. Mammarella, J. Bäck, J. Rinne, T. M. Ruuskanen, P. Hari, T. Vesala and M. Kulmala, Ozone deposition into a boreal forest over a decade of observations: evaluating deposition partitioning and driving variables, *Atmos. Chem. Phys.*, 2012, **12**, 12165–12182, DOI: 10.5194/acp-12-12165-2012.

27 R. Oswald, M. Ermel, K. Hens, A. Novelli, H. G. Ouwersloot, P. Paasonen, T. Petäjä, M. Sipilä, P. Keronen, J. Bäck, R. Königstedt, Z. Hosaynali Beygi, H. Fischer, B. Bohn, D. Kubistin, H. Harder, M. Martinez, J. Williams, T. Hoffmann, I. Trebs and M. Sörgel, A comparison of HONO budgets for two measurement heights at a field station within the boreal forest in Finland, *Atmos. Chem. Phys.*, 2015, **15**, 799–813, DOI: 10.5194/acp-15-799-2015.

28 H. Meusel, U. Kuhn, A. Reiffs, C. Mallik, H. Harder, M. Martinez, J. Schuladen, B. Bohn, U. Parchatka, J. N. Crowley, H. Fischer, L. Tomsche, A. Novelli, T. Hoffmann, R. H. H. Janssen, O. Hartogensis, M. Pikridas, M. Vrekoussis, E. Bourtsoukidis, B. Weber, J. Lelieveld, J. Williams, U. Pöschl, Y. Cheng and H. Su, Daytime formation of nitrous acid at a coastal remote site in Cyprus indicating a common ground source of atmospheric HONO and NO, *Atmos. Chem. Phys.*, 2016, **16**, 14475–14493, DOI: 10.5194/acp-16-14475-2016.

29 R. Rynek, T. Mayer and H. Borsdorf, Enhancing forest air sampling using a novel reusable ozone filter design, *Atmos. Meas. Tech.*, 2025, **18**, 4103–4117, DOI: 10.5194/amt-18-4103-2025.

30 C. M. Nussbaumer, U. Parchatka, I. Tadic, B. Bohn, D. Marno, M. Martinez, R. Rohloff, H. Harder, F. Kluge, K. Pfeilsticker, F. Obersteiner, M. Zöger, R. Doerich, J. N. Crowley, J. Lelieveld and H. Fischer, Modification of a conventional photolytic converter for improving aircraft measurements of NO2 via chemiluminescence, *Atmos. Meas. Tech.*, 2021, **14**, 6759–6776, DOI: 10.5194/amt-14-6759-2021.

31 J. M. Liebmann, J. B. A. Muller, D. Kubistin, A. Claude, R. Holla, C. Plass-Dülmer, J. Lelieveld and J. N. Crowley, Direct measurements of NO3 reactivity in and above the boundary layer of a mountaintop site: identification of reactive trace gases and comparison with OH reactivity, *Atmos. Chem. Phys.*, 2018, **18**, 12045–12059, DOI: 10.5194/acp-18-12045-2018.

32 P. Dewald, S. T. Andersen, G. N. T. E. Türk, L. Wüst, A. C. Nelson, J. Schuladen, U. Parchatka, M. Ehn, I. Mammarella, H. Fische, J. Lelieveld and J. N. Crowley, Vertical profiles of NO3 reactivity within the surface layer of a boreal forest, *Environ. Sci.: Atmos.*, 2025, DOI: 10.1039/D5EA00153F.

33 R. Dörich, P. Eger, J. Lelieveld and J. N. Crowley, Iodide CIMS and m/z 62: the detection of HNO_3 as NO_3^- in the presence of PAN, peroxyacetic acid and ozone, *Atmos. Meas. Tech.*, 2021, **14**, 5319–5332, DOI: 10.5194/amt-14-5319-2021.

34 Y. Ji, L. G. Huey, D. J. Tanner, Y. R. Lee, P. R. Veres, J. A. Neuman, Y. Wang and X. Wang, A vacuum ultraviolet ion source (VUV-IS) for iodide–chemical ionization mass spectrometry: a substitute for radioactive ion sources, *Atmos. Meas. Tech.*, 2020, **13**, 3683–3696, DOI: 10.5194/amt-13-3683-2020.

35 P. Warneck and T. Zerbach, Synthesis of peroxyacetyl nitrate in air by acetone photolysis, *Environ. Sci. Technol.*, 1992, **26**, 74–79.

36 F. M. Flocke, A. J. Weinheimer, A. L. Swanson, J. M. Roberts, R. Schmitt and S. Shertz, On the measurement of PANs by gas chromatography and electron capture detection, *J. Atmos. Chem.*, 2005, **52**, 19–43.

37 A. D. Awtrey and R. E. Connick, The absorption spectra of I_2, I_3^-, I^-, IO_3^-,$S_4O_6^-$ and $S_2O_3^-$. Heat of the reaction $I_3^- = I_2 + I^-$, *J. Am. Chem. Soc.*, 1951, **73**, 1842–1843, DOI: 10.1021/ja01148a504.

38 M. Berasategui, D. Amedro, L. Vereecken, J. Lelieveld and J. N. Crowley, Reaction between CH3C(O)OOH (peracetic acid) and OH in the gas phase: a combined experimental and theoretical study of the kinetics and mechanism, *Atmos. Chem. Phys.*, 2020, **20**, 13541–13555, DOI: 10.5194/acp-20-13541-2020.

39 O. Peltola, K. Lapo and C. K. Thomas, A Physics-Based Universal Indicator for Vertical Decoupling and Mixing Across Canopies Architectures and Dynamic Stabilities, *Geophys. Res. Lett.*, 2021, **48**, e2020GL091615, DOI: 10.1029/2020GL091615.

40 K. Pilegaard, Processes regulating nitric oxide emissions from soils, *Philos. Trans. R. Soc., B*, 2013, **368**, ARTN20130126, DOI: 10.1098/rstb.2013.0126.

41 J. A. Garland and S. A. Penkett, Absorption of peroxy acetyl nitrate and ozone by natural surfaces, *Atmos. Environ.*, 1976, **10**, 1127–1131, DOI: 10.1016/0004-6981(76)90122-0.

42 A. C. Hill, Vegetation: A Sink for Atmospheric Pollutants, *J. Air Pollut. Control Assoc.*, 1971, **21**, 341–346, DOI: 10.1080/00022470.1971.10469535.

43 C. K. Thomas, A. Serafimovich, L. Siebicke, T. Gerken and T. Foken, in *Energy and Matter Fluxes of a Spruce Forest Ecosystem*, ed. T. Foken, Springer International Publishing, Cham, 2017, pp. 113–135, DOI: 10.1007/978-3-319-49389-3_6.

44 W. Schrimpf, K. Lienaerts, K. P. Muller, J. Rudolph, R. Neubert, W. Schussler and I. Levin, Dry deposition of peroxyacetyl nitrate (PAN): Determination of its deposition velocity at night from measurements of the atmospheric PAN and (222)Radon concentration gradient, *Geophys. Res. Lett.*, 1996, **23**, 3599–3602, DOI: 10.1029/96gl03287.

45 P. Keronen, A. Reissell, Ü. Rannik, T. Pohja, E. Siivola, V. Hiltunen, P. Hari, M. Kulmala and T. Vesala, Ozone flux

measurements over a scots pine forest using eddy covariance method:: performance evaluation and comparison with flux-profile method, *Boreal Environ. Res.*, 2003, **8**, 425–443.

46 C. Hardacre, O. Wild and L. Emberson, An evaluation of ozone dry deposition in global scale chemistry climate models, *Atmos. Chem. Phys.*, 2015, **15**, 6419–6436, DOI: 10.5194/acp-15-6419-2015.

47 R. Sander, Compilation of Henry's law constants (version 5.0.0) for water as solvent, *Atmos. Chem. Phys.*, 2023, **23**, 10901–12440, DOI: 10.5194/acp-23-10901-2023.

48 A. Finco, M. Coyle, E. Nemitz, R. Marzuoli, M. Chiesa, B. Loubet, S. Fares, E. Diaz-Pines, R. Gasche and G. Gerosa, Characterization of ozone deposition to a mixed oak–hornbeam forest – flux measurements at five levels above and inside the canopy and their interactions with nitric oxide, *Atmos. Chem. Phys.*, 2018, **18**, 17945–17961, DOI: 10.5194/acp-18-17945-2018.

49 M. Ammann, R. A. Cox, J. N. Crowley, H. Herrmann, M. E. Jenkin, V. F. McNeill, A. Mellouki, M. J. Rossi, J. Troe and T. J. Wallington. Task Group on Atmospheric Chemical Kinetic Data Evaluation, IUPAC, Last access Sept. 2025, https://iupac.aeris-data.fr/.

50 J. Liebmann, E. Karu, N. Sobanski, J. Schuladen, M. Ehn, S. Schallhart, L. Quéléver, H. Hellen, H. Hakola, T. Hoffmann, J. Williams, H. Fischer, J. Lelieveld and J. N. Crowley, Direct measurement of NO_3 radical reactivity in a boreal forest, *Atmos. Chem. Phys.*, 2018, **2018**, 3799–3815, DOI: 10.5194/acp-18-3799-2018.

51 H. Hellén, A. P. Praplan, T. Tykkä, I. Ylivinkka, V. Vakkari, J. Bäck, T. Petäjä, M. Kulmala and H. Hakola, Long-term measurements of volatile organic compounds highlight the importance of sesquiterpenes for the atmospheric chemistry of a boreal forest, *Atmos. Chem. Phys.*, 2018, **18**, 13839–13863, DOI: 10.5194/acp-18-13839-2018.

52 K. Hens, A. Novelli, M. Martinez, J. Auld, R. Axinte, B. Bohn, H. Fischer, P. Keronen, D. Kubistin, A. C. Nolscher, R. Oswald, P. Paasonen, T. Petaja, E. Regelin, R. Sander, V. Sinha, M. Sipila, D. Taraborrelli, C. T. Ernest, J. Williams, J. Lelieveld and H. Harder, Observation and modelling of HOx radicals in a boreal forest, *Atmos. Chem. Phys.*, 2014, **14**, 8723–8747, DOI: 10.5194/acp-14-8723-2014.

53 J. Aalto, P. Aalto, P. Keronen, P. Kolari, P. Rantala, R. Taipale, M. Kajos, J. Patokoski, J. Rinne, T. Ruuskanen, M. Leskinen, H. Laakso, J. Levula, T. Pohja, E. Siivola, M. Kulmala, and I. Ylivinkka, *SMEAR II Hyytiälä Forest Meteorology, Greenhouse Gases, Air Quality and Soil (Version 4)*, 2025, Repository, doi: DOI: 10.23729/fd-933fd9fd-d31b-3e26-a01b-acef7901b843.